THEORETICAL AND EXPERIMENTAL PERFORMANCE ANALYSIS OF A SOLAR ASSISTED HEAT PUMP

A THESIS SUBMITTED TO
THE GRADUATE SCHOOL OF NATURAL AND APPLIED SCIENCES
OF
MIDDLE EAST TECHNICAL UNIVERSITY

BY

AHMET ÇAĞLAR

IN PARTIAL FULFILLMENT OF THE REQUIREMENTS
FOR
THE DEGREE OF MASTER OF SCIENCE
IN
MECHANICAL ENGINEERING

DECEMBER 2006

Approval of the Graduate School of Natural and Applied Sciences

_____

Prof. Dr. Canan Özgen

Director

I certify that this thesis satisfies all the requirements as a thesis for the degree of Master of Science.

_____

Prof. Dr. S. Kemal İder

Head of Department

This is to certify that we have read this thesis and that in our opinion it is fully adequate, in scope and quality, as a thesis for the degree of Master of Science.

_____

Assoc. Prof. Dr. Cemil Yamalı

Supervisor

Examining Committee Members

Prof. Dr. Kahraman Albayrak (METU, ME) _____

Assoc. Prof. Dr. Cemil Yamalı (METU, ME) _____

Asst. Prof. Dr. Cüneyt Sert (METU, ME) _____

Asst. Prof. Dr. Almila Yazıcıoğlu (METU, ME) _____

Asst. Prof. Dr. İbrahim Atılgan (Gazi Unv., ME) _____

I hereby declare that all information in this document has been obtained and presented in accordance with academic rules and ethical conduct. I also declare that, as required by these rules and conduct, I have fully cited and referenced all material and results that are not original to this work.

Name, Last name: Ahmet Çağlar

Signature :

ABSTRACT

THEORETICAL AND EXPERIMENTAL PERFORMANCE ANALYSIS OF A SOLAR ASSISTED HEAT PUMP

Çağlar, Ahmet

M.S., Department of Mechanical Engineering

Supervisor: Assoc. Prof. Cemil Yamalı

December 2006, 94 Pages

In this thesis, performance of a heat pump aided by solar heating system with an evacuated tubular collector has been analyzed theoretically and experimentally. For this purpose, a domestic hot water heating system has been designed, constructed and tested. The evacuated tubular solar collector has been used to achieve higher collector efficiency in winter. The fraction of the solar energy utilized has been measured experimentally and estimated theoretically. Effects of various parameters have been investigated on the performance of the proposed system.

A mathematical model was developed to investigate the effects of different environmental, design and operational parameters on the solar heating system. In order to compare the obtained theoretical results with experimental ones, an experimental study has been carried out. For that, a number of experiments have been made at the solar house of the Mechanical Engineering Department of METU. An air-to-air heat pump was integrated with an evacuated tubular solar water heater unit (closed water circulation) and the performance of it has been studied experimentally. As a result of the experimental study, the maximum value of the coefficient of performance of the solar assisted heat pump used in this study was obtained as 4.85. The second law efficiency of the system was between 4.8-27.4 %.

Keywords: Solar assisted heat pump; heat pump; evacuated tubular solar collector; solar radiation; vapor compression refrigeration cycle.

ÖZ

GÜNEŞ ENERJİSİ DESTEKLİ ISI POMPASI SİSTEM PERFORMANSININ DENEYSEL VE TEORİK OLARAK ANALİZİ

Çağlar, Ahmet
Yüksek Lisans, Makine Mühendisliği Bölümü
Tez Yöneticisi: Doç. Dr. Cemil Yamalı
Aralık 2006, 94 Sayfa

Bu çalışmada, vakum tipi kollektörlü bir güneş ısıtma sisteminin performansı teorik ve deneysel olarak incelendi. Bu amaç için domestik sıcak su ısıtma sistemi kuruldu ve test edildi. Tüp tipi solar kollektörler kullanılarak kışın daha yüksek verimler elde etmeye çalışıldı. Faydalı güneş enerjisi ölçülerek bulundu. Saatlik güneş radyasyonu teorik olarak da hesaplandı. Değişik parametrelerin sistem performansı üzerindeki etkileri araştırıldı. Farklı çevresel, tasarım ve çalışma parametrelerinin sistemin performansı üzerine olan etkilerini incelemek için matematik modele dayalı olan bir bilgisayar simülasyon programı geliştirildi.

Elde edilen teorik sonuçlar deneysel sonuçlarla karşılaştırıldı ve geliştirilen matamatiksel modelin deneysel sonuçlarla uyumu incelendi. Bu amaç için, deney düzeneği tasarlandı, imalatı yaptırıldı ve deneysel çalışmaya hazır hale getirildi. Deneyler ODTÜ Makina Mühendisliği bölümündeki güneş evinde yapıldı. Mevcut hava koşullandırıcılı ısıtma sistemi güneş evindeki vakumlu cam borulu su ısıtma sistemi ile entegre edilerek sistemin performansı deneysel olarak incelendi. Yapılan deneyler sonucunda kullanılan güneş destekli ısı pompasının maksimum performans katsayısı 4.85 olarak bulundu. Termodinamiğin ikinci kanun verimi ise % 4.8-27.4 arasında değişti.

Anahtar Kelimeler: Güneş enerjisi destekli ısı pompası; ısı pompası; vakumlu tip güneş kollektörü; güneş radyasyonu; buhar sıkıştırmalı soğutma çevrimi.

To my family

who always support me in all aspects of my life

ACKNOWLEDGEMENTS

I am deeply grateful to my supervisor, Assoc. Prof. Cemil YAMALI, for his guidance, inspiration, and invaluable help all throughout the study.

I gratefully acknowledge Mustafa Yalçın, for his technical assistance in manufacturing and operating the setup.

Finally, I offer sincere appreciation to my family, for their continuous encouragement, understanding, and support.

TABLE OF CONTENTS

LIST OF TABLES

LIST OF FIGURES

LIST OF SYMBOLS

A	Area, m^2
COP	Coefficient of performance
c_p	Specific heat at constant pressure, kJ/kgK
D	Diameter, m
F'	Collector efficiency factor
F_R	Heat removal factor
g	Gravitational acceleration, m/s^2
Gr	Grashof number
G_{sc}	Solar constant, 1367 W/m^2
H	Daily solar radiation, J/m^2
h	Enthalpy, kJ/kg
h_i	Inner convection heat transfer coefficient, W/m^2K
h_o	Outer convection heat transfer coefficient, W/m^2K
I	Total radiation on a horizontal surface, W/m^2
$I_{b,}\ I_d$	Beam and diffuse radiation, W/m^2
I_o	Hourly extraterrestrial radiation, J/m^2
I_T	Hourly total radiation on a tilted surface, J/m^2
k	Thermal conductivity, W/mK
k_T	Hourly clearness index
L	Height of the tank, coil length, m
N	Day length, h
m	Mass flow rate, kg/s
n	Number of day in a year
Nu	Nusselt number
P_{crit}	Critical pressure
Pr	Prandtl number
Q	Heat transfer rate, kW
Q_u	Useful solar gain, W

R	Thermal resistance, K/W
r	Radius, m
Ra	Rayleigh number
S	Absorbed radiation, W/m^2
T	Temperature, K
U	Overall heat loss coefficient, W/m^2K
U_L	Overall heat loss coefficient for the collector, W/m^2K
W	Work input, kW
w	Hour angle
w_s	Hour angle at sunset
Z	Zenith angle

Greek Symbols

α	Altitude angle, thermal diffusivity, m^2/s
$\tau\alpha$	Transmittance-absorptance product
ϕ	Solar azimuth angle
γ	Surface azimuth angle
ρ_g	Diffuse reflectance
v	kinematic viscosity, m^2/s
β	Thermal expansion coefficient, 1/K
η	Efficiency
μ	Dynamic viscosity, Pa.s

Subscripts

a	Ambient
ave	Average
c	Collector
f	Film (average)

i, o	Inner and outer
ins	Insulation
m	Mean
s	Storage
t	Tube
w	Water

CHAPTER 1

INTRODUCTION

The development of social life standards and increase in civilization level of the humanity as well as industrialization bring about to increase in energy demands. After energy production started with the use of coal and oil as fuel, gas based plants were used. Thereby it was tried to meet the demands. However, exhausts of these fuels have caused to the pollution of the atmosphere dramatically. The combustion of fossil fuels has carried the pollution to unacceptable levels.

Over the last decade, concerns regarding limited oil and gas reserves, global warming and ozone depletion have made necessary the usage of clean and renewable energy resources. Governments and industry all around the world have started to invest in alternative energy resources.

Nowadays, 88% of the total commercial energy demand is achieved by fossil fuels and the rest by nuclear and hydraulic resources. Alternative energy resources must take their place in proportion. One of the most important alternative energy resources is solar energy. Solar energy is also the main source of fossil fuels, hydraulic and wind energy.

Solar energy is mainly used to heat residence, greenhouse and domestic water. It is also used to produce hydrogen and electricity.

1.1 Definition of Heat Pump

Heat is transferred from high-temperature media to low-temperature media without requiring any device. But, to perform the reverse process, some devices are

needed. Heat pumps and refrigerators are devices that receive heat from a lower temperature reservoir and reject it to a higher temperature reservoir. Heat pump has the same cycle with a refrigerator that is commonly used in residences. The difference in between a refrigerator and a heat pump is only the purpose. Refrigerators are intended for cooling a selected space by extracting heat at lower temperature. If desired effect is to heat the space, heat is discharged at higher temperature in heat pumps.

A heat pump can either extract heat from a heat source and reject heat to air and water at a higher temperature for heating, or provide refrigeration at a lower temperature and reject condensing heat at a higher temperature for cooling. During summer, the heat extraction, or refrigeration effect, is the useful effect for cooling in a heat pump. In winter, the rejected heat provides heating in a heat pump [1].

Heat pumps provide both energy-efficient and cost-efficient solution to the demand for heating. The most important advantage of this type of heating system is that more energy can be available for space heating than the work required to operate a heat pump. In fact, modern electrical heat pumps can achieve performance factors (coefficient of performance, COP) between 3.5 and 5.5. This means that for every kWh power consumption, 3.5 to 5.5 kWh heating energy can be created [2]. Addition to this high performance advantage, causing less pollution, the ability to make both heating and cooling and the feasibility for industrial applications have increased the popularity of heat pumps.

1.2 The Reversed Carnot Cycle

The Carnot cycle is a totally reversible cycle and it is composed of two reversible isothermal and two reversible adiabatic (isentropic) processes. The theoretical heat engine that operates on the Carnot cycle is called the Carnot heat engine and the reverse cycle of it is called the Carnot refrigeration cycle [3].

A heat engine receives heat from high temperature reservoir and produces work by

rejecting that heat to low temperature reservoir. Maximum theoretical work that a heat engine can produce is achieved by Carnot cycle. Consequently, the maximum possible efficiency of a cycle can be obtained from the Carnot cycle between same temperature reservoirs according to the Carnot principles. Figure 1.1 shows the P-ν and T-s diagrams of a reversed Carnot cycle.

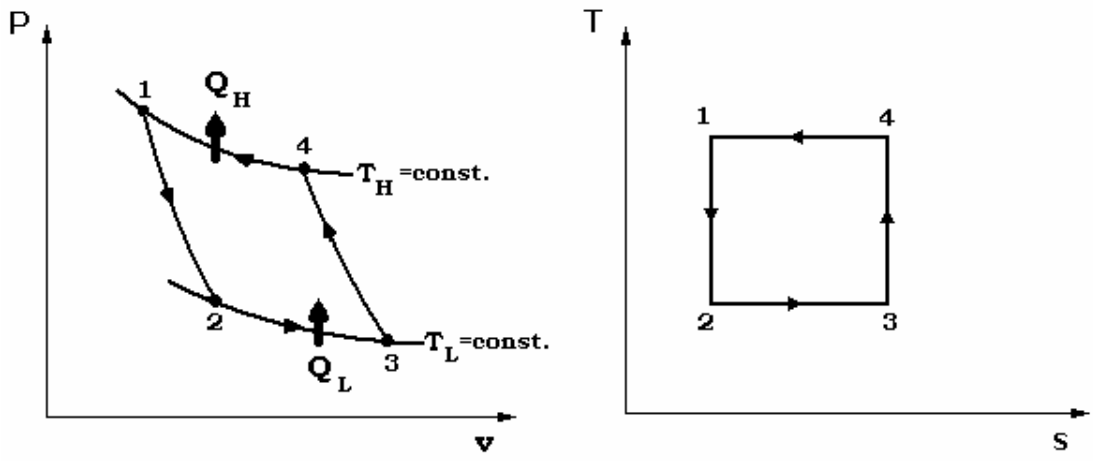

Figure1.1 P-ν and T-s diagrams of a reversed Carnot cycle.

The four reversible processes are as follows:

1-2 Reversible adiabatic (isentropic) expansion: The temperature of the working fluid which is at T_H temperature drops to T_L temperature isentropically.
2-3 Reversible isothermal heat absorption: Heat is transferred isothermally from the low-temperature source at T_L temperature to the working fluid in the amount of Q_L.
3-4 Reversible adiabatic (isentropic) compression: The working fluid is compressed isentropically by doing work on the system. The temperature of the fluid increases from T_L temperature to its initial T_H temperature.
4-1 Reversible isothermal heat rejection: The working fluid rejects heat at constant T_H temperature to the high-temperature reservoir in the amount of Q_H.

A work done on the system is needed to keep the temperature of the space above the

atmospheric temperature. According to the Clausius statement in thermodynamics, *it is impossible to construct a device that operates in a cycle and produces no effect other than the transfer of heat from a lower temperature body to a higher temperature body*. That is, heat cannot be transferred from a lower temperature medium to a higher temperature medium without an input of work.

The coefficient of performance of a heat pump is the ratio of the desired output Q_H to required input W_{net} $(Q_H - Q_L)$ by definition:

$$COP_{HP} = \frac{desired\ output}{required\ input} = \frac{Q_H}{Q_H - Q_L} = \frac{Q_H}{W_{in}} \tag{1.1}$$

Since energy reservoirs are characterized by their temperatures, the coefficient of performance of a reversible heat pump (Carnot heat pump) is a function of the temperatures only and becomes:

$$COP_{HP,Carnot} = \frac{T_H}{T_H - T_L} \tag{1.2}$$

This is the highest value that a heat pump operating between the temperature limits of T_L and T_H can have [3].

1.3 The Ideal Vapor Compression Refrigeration Cycle

The working fluid (refrigerant) is vaporized completely before compression on the ideal vapor compression refrigeration cycle since the existence of liquid in vaporized refrigerant entering a compressor can damage the valves. The turbine on Carnot cycle replaces with a throttling device, such as expansion valve or capillary tube. This cycle is the most widely used cycle for refrigerators, air conditioning systems and heat pumps. Schematic and T-s diagrams of an ideal vapor compression refrigeration cycle are shown in Figure 1.2. It consists of four processes [3]:

1-2 Isentropic compression in compressor

2-3 Constant pressure heat rejection in condenser

3-4 Throttling in an expansion device

4-1 Constant pressure heat absorption in an evaporator

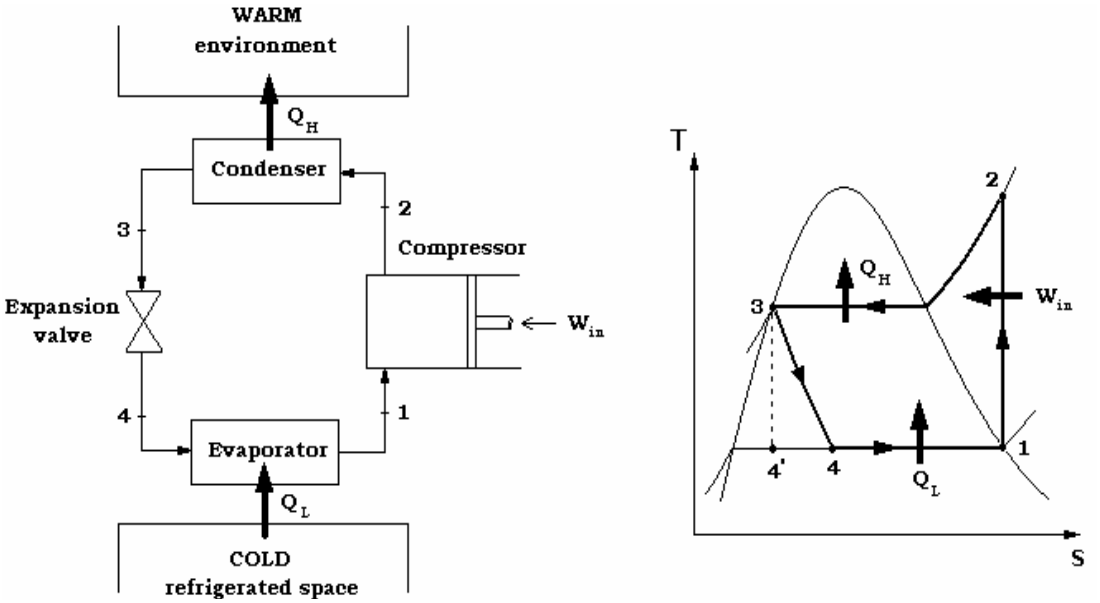

Figure 1.2 Schematic and T-s diagram for the ideal vapor compression refrigeration cycle.

The refrigerant enters the compressor at state 1 as saturated vapor with low pressure and temperature and is compressed isentropically to the condenser pressure. The temperature of the refrigerant increases during this isentropic compression process to well above the temperature of the surrounding medium, such as atmospheric air. Then the refrigerant enters the condenser as superheated vapor at state 2 and leaves as saturated liquid at state 3 by rejecting heat to high temperature medium (the surroundings).

The pressure of the saturated liquid refrigerant at state 3 drops to the evaporator pressure by passing through an expansion valve or capillary tube. The temperature of the refrigerant drops below the temperature of the refrigerated space during this

process. The refrigerant enters the evaporator at state 4 as a low-quality saturated mixture and it evaporates completely by absorbing heat from the refrigerated space. The refrigerant leaves the evaporator as saturated vapor and enters the compressor. Therefore, the cycle is completed [3].

The ideal vapor compression refrigeration cycle is not an internally reversible cycle because it involves an irreversible throttling process.

Another diagram frequently used in the analysis of vapor compression refrigeration cycle is the P–h diagram, as shown in Figure 1.3.

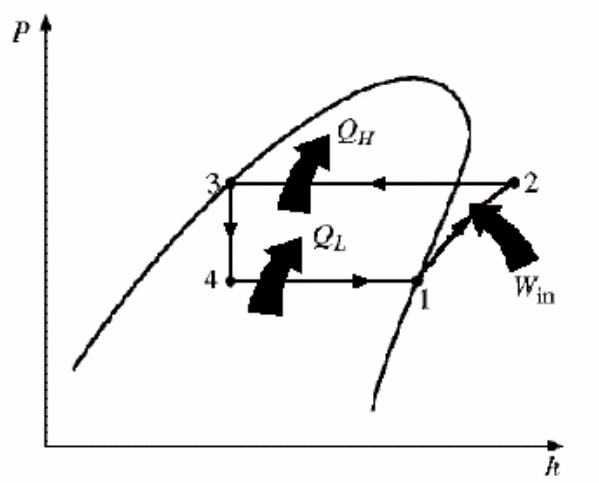

Figure 1.3 P-h diagram of ideal vapor compression refrigeration cycle.

The coefficient of performance of heat pumps operating on the ideal vapor compression refrigeration cycle can be expressed as:

$$COP = \frac{q_h}{w_{net,in}} = \frac{h_2 - h_3}{h_2 - h_1} \tag{1.3}$$

where, h denotes enthalpy values of corresponding states, q_h is heat rejected at condenser and $w_{net,in}$ is work input to the system.

1.4 Actual Vapor Compression Refrigeration Cycle

Actual vapor compression refrigeration cycle deviates from the ideal cycle due to irreversibilities. Two common reasons for irreversibilities are fluid flow, which causes pressure drops and heat transfers. T-s diagram of an actual vapor compression refrigeration cycle is shown in Figure 1.4.

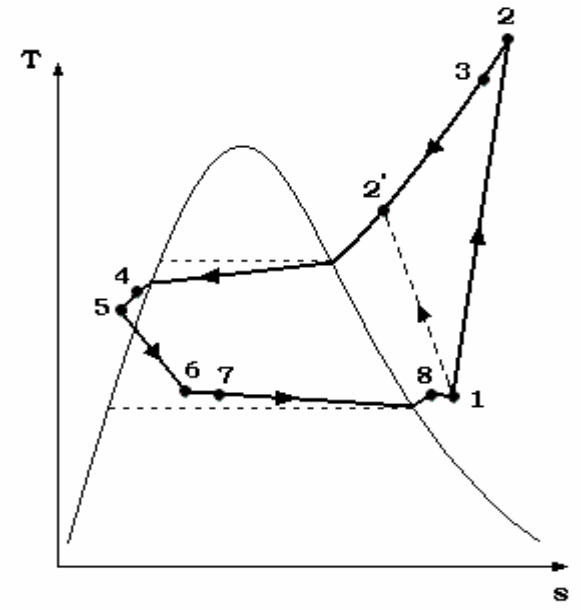

Figure 1.4 T-s diagram of the actual vapor compression refrigeration cycle.

The refrigerant enters the compressor as slightly superheated instead of saturated vapor. Furthermore, the piping between the evaporator and the compressor is very long, thus a significant heat transfer from the surroundings and a pressure drop caused by fluid friction occur along the piping. There is also a pressure drop in the evaporator. These three deviations from the ideal cause an increase in specific volume of the refrigerant and thus an increase in the power requirements to the compressor.

The compression process, which is assumed to be isentropic in the ideal cycle, may have an increase or decrease in entropy. At the compressor inlet, the refrigerant has

lower temperature than the compressor cylinder wall and therefore heat is transferred to the refrigerant. In the same way, heat is transferred from the refrigerant at the compressor exit because the temperature of the refrigerant is higher than the compressor temperature. Therefore, an increase in entropy occurs at the beginning of the compression and a decrease in entropy at the end of it.

It is difficult to realize a constant pressure process at the condenser since there is a pressure drop. Therefore, the temperature of the refrigerant becomes lower than the saturation temperature and the refrigerant enters the throttling valve as subcooled. A pressure drop also occurs in the piping between the condenser and the throttling valve.

Overall COP of a system that includes more applications than a heat pump like solar assisted heat pump can be calculated by following relation:

$$COP_{overall} = \frac{Q_H}{W_{comp} + W_{fan} + W_{others}} \tag{1.4}$$

Log-h diagram of an actual vapor compression cycle is shown in Figure 1.5.

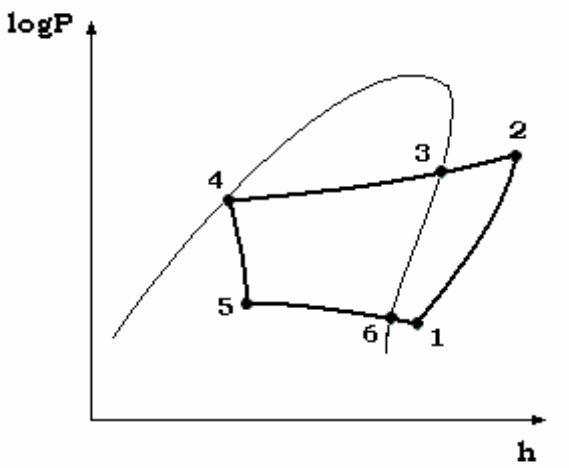

Figure 1.5 Real process of a vapor compression heat pump cycle.

The changes of states, which deviate from ideal process, can be described as follows:

1-2 Compression with a variable polytropic exponent
2-3 Heat output with loss of pressure due to friction
3-4 Heat output by condensation with loss of pressure
4-5 Expansion with heat input
5-1 Heat input with loss of pressure and superheating [4]

1.5 Refrigerants

A number of refrigerants are used in vapor compression refrigeration cycles. Ammonia and sulfur dioxide were first used as vapor compression refrigerants. Today, the main refrigerants are the halogenated hydrocarbons, which are marketed under trade names such as Freon, Genetron, Suva and so on. Two important parameters in selecting a refrigerant are the temperatures of the two media (the refrigeration space and the environment) with which the refrigerant exchanges heat and the type of the equipment to be used [5].

The main refrigerants that are now used in heat pumps are listed in table 1.1 together with following important properties related to a condensing temperature of +50 ^{0}C and an evaporation temperature of 0 ^{0}C:

a) The ideal COP as a theoretical value
b) The volumetric heat output Q_H, which is defined as the ratio of the heat flow Q at the condenser to the volume flow V_0 delivered by the compressor.
c) The condensing pressure P at a condensing temperature of +50 ^{0}C. The higher the pressure, the more expensive are the components which have to withstand this pressure.
d) The pressure ratio P/P_0 of the condensing pressure at T=+50 ^{0}C and the evaporation pressure at T_0=0 ^{0}C. The lower this ratio, the higher volumetric efficiency of the compressor can be achieved [5].

A temperature difference of 10 ^{0}C or more should be maintained between the refrigerant and the medium to have a reasonable heat transfer rate. The evaporation pressure, which is the lowest pressure in a refrigeration cycle, should be above the atmospheric pressure to prevent any air leakage into the system. Therefore, a refrigerant should have a saturation pressure of 1 atm or higher at its evaporation temperature. The temperature of the refrigerant in the condenser cannot fall below the temperature of the cooling medium and the saturation pressure of the refrigerant and this temperature should be below its critical pressure to reject heat as approximately isothermal [3].

Table1.1. Parameters of various refrigerants at a condensing temperature of 50 ^{0}C and an evaporating temperature of 0 ^{0}C.

Refrigerant	*Ideal COP*	*Volumetric heat output* Q_H (kj/m^3)	*Pressure ratio* P/P_0	*Condensing pressure* P (bar)
R 11	5,53	443	5,88	2,4
R 12	5,16	2290	3,96	12,2
R 12B1	5,74	1075	4,75	5,6
R 21	4,64	636	5,68	4,0
R 22	5,14	3761	3,88	19,3
R 114	4,61	784	5,06	4,5
RC 318	4,53	1163	5,12	6,7
R 502	4,35	3676	3,68	21,1
NH3	5,53	4275	4,96	20,6

Other desirable characteristics of a refrigerant include being nontoxic, noncorrosive, nonflammable, and chemically stable; having a high enthalpy of vaporization; and being with low cost [3].

1.6 Heat Sources

The type of the building, climatic conditions and the location of the proposed system determine the advantages of a design. Another important criterion is the heat source chosen because the temperature of the heat source and the constancy of the

temperature affect both the heat characteristics such as the coefficient of performance and the economics.

An ideal heat source is inexpensive, abundant and it has a temperature as high as possible. The difference should be small between the desired temperature and the temperature of available heat source. In addition, the heat transfer medium should not affect the heat exchange equipment chemically and physically (corrosion, contamination, freezing).

The usage of heat pump alone may not be economical at very low temperatures of the heat source. Auxiliary heat sources should be used in such a case.

Heat sources, which are directly derived from the nature, are called natural heat sources. An essential feature of these heat sources is that they derive their heat from normal climatic phenomena. Natural heat sources all have temperatures more or less dependent on the seasons, the greater the heat capacity of the source the less the temperature variation [4]. The main natural heat sources are air, water and soil.

1.6.1 Air

Air is the most common source in practice and it offers the possibility of a substantially universal heat source. However, there are a number of problems associated with its use as a heat source although air is free and widely available. Many localities experience not only wide fluctuations in air temperature, but also the temperature as the heating requirements increase. This will adversely affect the coefficient of performance and the size of the refrigeration system. In the cooler and more humid climates, some residual frost tends to accumulate on the outdoor heat transfer coil (evaporator) as the temperature falls below the 2-5 ^{0}C range, leading to a reduction in the capacity of the heat pump. As the heating load is greatest at the lowest temperature, a supplementary heating source is required. This device could be an existing oil, gas or electric furnace or electric resistance heating; the latter is usually part of the heat pump system [7].

1.6.2 Water

Because of its high heat capacity and good heat transfer properties, water is the best heat source. Water from wells, lakes, rivers, and wastewaters meets to requirements. Water-source units are common in applied or built-up installations where internal heat sources, heat or cold reclaim is possible. In addition, solar or off-peak thermal storage systems can be used [4, 5, 7].

Surface water, rivers and lakes can be used as a heat source. They suffer from the major disadvantage that the source either freezes in winter or the temperature can be very close to 0 ^{0}C (typically 2-4 ^{0}C). As a result, great care is needed to avoid freezing on the evaporator. Many rivers are warmed up by wastewater, from industrial cooling water or power stations, to such an extent that they no longer freeze [4, 5].

Ground water, i.e. water at depth of up to 80 meters, is available in most areas with temperatures generally in the 5-18 ^{0}C range. One of the main difficulties with these sources is that often the water has a high dissolved solids content producing fouling or corrosion problems with heat exchangers [5].

Water-to-air heat pump uses water as a heat source and uses air to move the heat to or from the conditioned space. Almost any water can be used as the source: river water, lake water, ground or well water, wastewater, and so on.

1.6.3 Soil

Soil is very suitable heat source because of its high and constant temperature, availability and storage capacity. Generally, the heat can be extracted from pipes laid horizontally or sunk vertically in the soil. The latter system appears to be suitable for larger heat pump systems.

Due to the removal of heat from the soil, the soil temperature may fall during the heating season. Depending on the depth of the coils, recharging may be necessary during the warm months to raise the ground temperature to its normal levels. This can be achieved by passive (e.g., solar irradiation) or active means [5].

1.7 Solar Energy and Solar Assisted Heat Pumps

Solar energy can be converted into mechanical energy or electricity energy. It is also used with a mechanical refrigeration cycle. Cost-effective and high-efficient collectors are essential for the widespread use of solar energy for heating and cooling of buildings and for agricultural and industrial processes. It is possible to construct a solar assisted heat pump with only small modifications by adding solar collector and storage system to a heat pump.

The great advantage of the use of solar assisted heat pump is that solar energy provides heat at a higher temperature level as a heat source than other sources. Thus, the coefficient of performance (COP) of a heat pump can be increased. Furthermore, the temperature of the collector can be reduced to the ambient temperature and, therefore, the heat loss to air can be reduced sufficiently. Diffuse indirect radiation can be used even with overcast skies and in the early and late of the day with the lower collector temperature. Thus, the collector efficiency and capacity can be increased. The great disadvantage of using the solar energy is that large areas are needed for large amounts of the solar radiation.

Solar assisted heat pumps have been concerned with two basic types of systems in researching and development, direct and indirect. Solar collector also serves as the evaporator of the heat pump in direct systems. Flat-plate type of solar collector is usually used. The collector surface can function to extract heat from the outdoor air when the collector has no glass cover plates. The same surface also serves as a condenser using outside air as a heat sink for cooling applications. Indirect systems employ another fluid, either water or air, which is circulated through the solar collector. The collector is used as an outdoor air preheater or the outdoor air loop can

be closed when air is used. These are air-to-air heat pumps. When water is circulated through the collector, either water-to-air or water-to-water type heat pumps are used.

Heat pumps complement solar collectors and heat storage in solar assisted heat pump systems in several ways [5]:

- Heat pumps are more efficient and can provide more heat for a given heat pump size if their evaporators can operate from a warm source. Thermal energy storage, heated by solar collectors, can provide that warming.
- Solar collectors operate more efficiently if they collect heat at lower temperatures. If the collected heat can be stored at a lower temperature because it is used to warm the evaporator of a heat pump, the collector is more efficient, and therefore less collector area is needed to collect a required amount of heat.
- Heat pumps are the most efficient way to use electricity for backup heat for a solar heating system, even if there is no direct thermal connection of the heat pump with the solar collector and storage system.
- Heat pumps can allow sensible-heat storage units (water, rock beds) to operate over wide temperature ranges, because stored heat down to 5 ^{0}C can be used in conjunction with heat pumps to heat a building.

Solar heating systems must be more economical for its common use and commercial viability in comparison with alternative nonsolar heating systems. An economic analysis should be made between the high first cost of solar heating and cooling equipment and the cost savings obtained by reducing the use of fuel or electricity. For instance, the comparison of the cost of electricity can be made between the nonsolar and solar heating system as they have same overall life-cycle cost.

There are several combinations of solar assisted heat pumps as shown in Figure 1.6. A parallel system uses solar energy in the heat exchanger first and then uses the air-to-air heat pump when the solar energy is unable to provide the necessary heat. A series system uses the solar energy in the heat exchanger first and then uses the water-to-air heat pump when the solar energy is unable to provide the necessary heat.

A dual-source system has the choice of either an air-heated coil when warm air is available or a water-heated coil when warm water is available.

A solar assisted heat pump saves the operating cost up to 20% during heating season compared to air-to-air heat pump. The COP value can reach to above 3. The energy required by electrical resistance heating can be saved up to 50% in parallel systems, up to 60% in series systems, and up to 70% in dual-source systems.

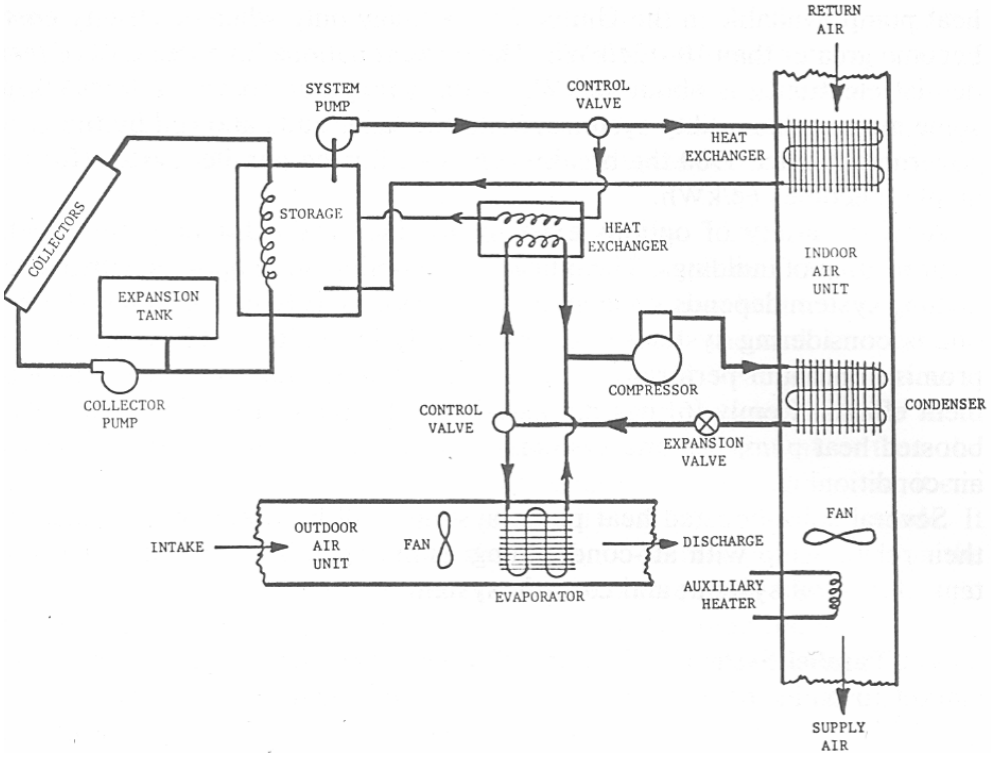

Figure 1.6 Solar assisted heat pump combinations.

1.7.1 Parallel System

Figure 1.7(a) shows a simple parallel system. The collector heats water if radiation is available and hot water is stored in a tank. Water in the tank is circulated through a water-to-air heat exchanger to heat the inside air. If the temperature of the water in the tank drops below a certain temperature (40 ^{0}C), an air-to-air heat pump is driven

by a controller to heat the house in the conventional way. Air-conditioning can be made in this system.

1.7.2 Series System

A series system is shown in Figure 1.7(b). The collector heats the water and this water is stored in a tank. The hot water is sent directly to the house if the water has enough energy to heat. The heat pump takes heat from the water in the tank and rejects heat to the house if solar energy is not sufficient to heat the house. The collector operates with high efficiency in this system because the tank can be operated at lower temperatures. In addition to this advantage, heat storage capacity of the tank can be increased by the amount of sensible heat stored. The disadvantage of this system is that the water under a certain temperature (5 ^{0}C) can freeze and this can damage the heat pump.

It is impossible to provide air-conditioning with a simple series system because there is no way to exhaust the waste heat to outside air. That can be possible if there were another heat exchanger loop between the storage tank and outside air, but this brings about extra costs [5].

1.7.3 Dual-source System

A dual system that is illustrated in Figure 1.7(c) combines the advantages of the parallel and the series systems and overcomes their disadvantages. The solar collector, heat storage, and building heat exchanger all continue to work as simple solar system as long as the tank temperature remains about 40 C. At temperatures below that, a microprocessor controller calls upon the heat pump system, and a decision is made as to whether it is better to draw the heat pump's heat from the tank or from the outside air. The control strategy options are numerous for this system: it can be operated to optimize savings of electricity or to reduce peak loads. It would be the most efficient of all systems described before. It has the disadvantage that required heat pump is complex and will be costly manufacture [5].

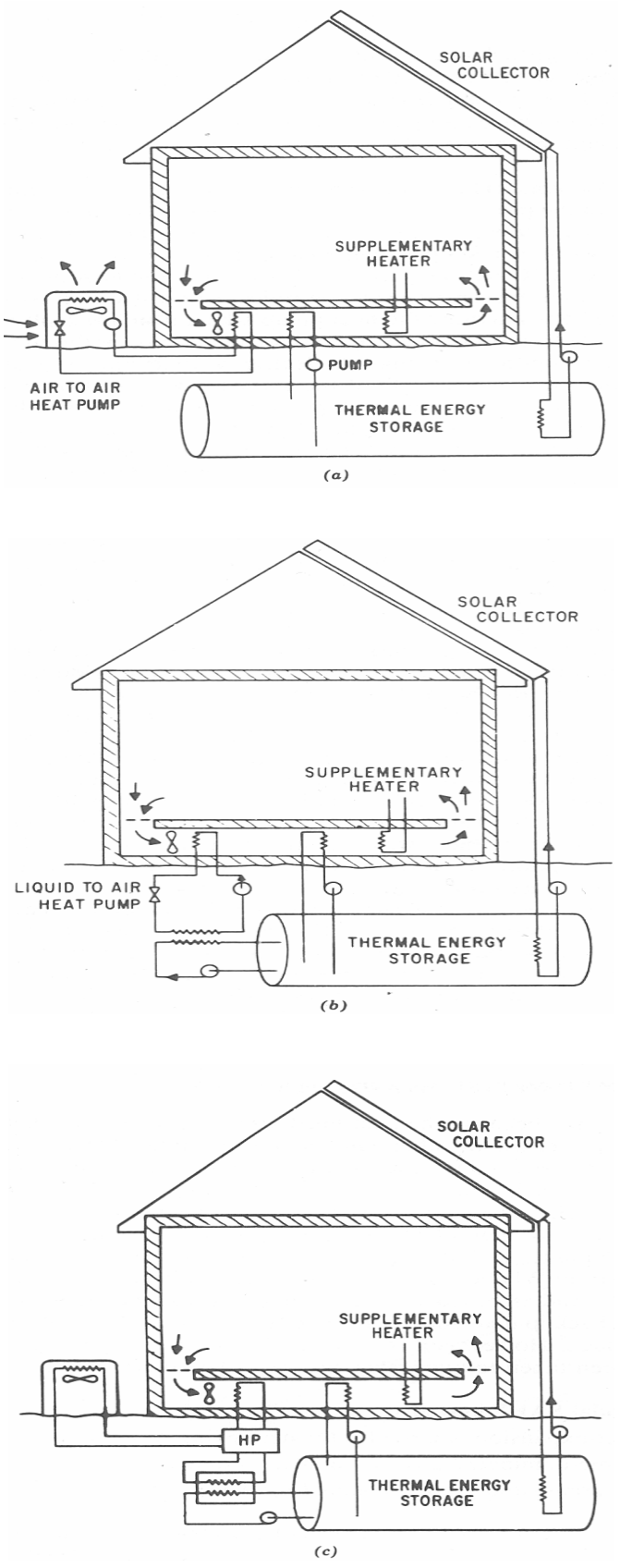

Figure 1.7 Schematic views of (a) parallel, (b) series, (c) dual systems.

1.8 Present Study

In this study, experimental and theoretical performance analysis of a solar assisted heat pump has been carried out. The main purpose of the study is to investigate the variations of the performance characteristics of the solar assisted heat pump with different temperatures of a storage tank. An experimental setup was constructed at the Department of Mechanical Engineering in Middle East Technical University.

The experiments were made in Ankara (40 ^{o}N, 33 ^{o}E), Turkey during the period of 8-23 of November 2006. Necessary parameters and climatic conditions were measured by various measurement devices. The experimental analysis was also supported by a theoretical analysis. A simple mathematical model was developed for this purpose.

In following chapters, a literature survey is made in Chapter 2. Chapter 3 contains the theoretical study and necessary calculations for both the solar energy system and the heat pump system. Energy balance and heat transfer phenomena in the storage tank are defined in this chapter. Chapter 4 presents the experimental study, the descriptions of the designed system and measurement devices, and the results of the experiments. The results are also figured out in this chapter. Chapter 5 gives a conclusion for the results and analysis of the system performance at the end of the study.

CHAPTER 2

LITERATURE SURVEY

During the last two decades, a number of investigations have been conducted by some researchers in the design, modeling and testing of solar assisted heat pump systems (SAHPS). These studies undertaken on a system basis may be categorized into four groups as follows [9]:

i. SAHPS for water heating,
ii. SAHPS with storage (conventional type) for space heating,
iii. SAHPS with direct expansion for space heating,
iv. Solar assisted ground source heat pump greenhouse heating system.

Yamankaradeniz and Horuz [10] were investigated the characteristics of a solar assisted heat pump theoretically and experimentally. They saw at the last of eight-month time period that in the coldest months collector efficiency and COP values decreased since the ambient temperature and solar radiation decreased drastically. Theoretical model were in good agreement with experimental results.

Huang and Chyng [11] used an integrated storage tank and Rankine cycle unit to make a more compact size. A thermosyphon loop was used to transfer heat from the condenser to the water storage tank, thus no circulation pump was needed. They found that with increasing solar radiation COP of the Rankine cycle first increases and reaches the maximum value of it and then starts to decrease. The effect of ambient temperature on the COP value is small. The highest COP value was 3.83. The evaporation temperature of Rankine cycle was 10 to 16 ^{0}C below the ambient temperature as a different manner.

Cervantes and Torres-Reyes [12] tested a direct expansion solar assisted heat pump where the collector acted as the evaporator of the heat pump. The reason for this arrengement is based on the steady state modeling of the thermodynamic cycle and the optimization of the exergy consumption (minimization of entropy generation). It is possible to increase the efficiency of the thermodynamic cycle by reducing the temperature difference between the actual and optimum evaporator temperature by means of an automatic control mechanism which regulates the condenser temperature to an optimum temperature. The analysis in this thermodynamical optimization study can be used for thermodynamical design of similar systems for a given set of conditions.

Ozgener and Hepbasli [13] established an experimental system to heat a greenhouse by using a solar assisted heat pump which used geothermal energy as an other source. They connected the geothermal energy application to the solar collector. Performance of the system mainly depends on the heat pump unit, circulation or well pumps and ground heat exchanger. Experimental results showed that such a system can be used in the Mediterranean and Aegean regions of Turkey. However, this system cannot meet overall heat loss of the greenhouse if the ambient temperature is very low.

Hulin et al. [14] tried two different configurations on their setup. As a first scheme, the evaporator of the heat pump is used as a collector always open to the atmosphere. Second sheme is designed in such a way that the evaporator was placed in a novel fresh water solar pond/tank. Thus, the COP of the heat pump can be increased in the second scheme since the water temperature in the tank is higher than the ambient temperature.

Abou-Ziyan et al. [15] made experiments by using different working fluids, R22, R134a and R404a, in their system at four different modes of operation: Mode 1. The conventional heat pump (solar air heater is omitted), Mode 2. Series solar assisted heat pump in which heated air flows from the solar collector to the evaporator then goes to the condenser, Mode 3. Series solar assisted heat pump in which heated air

flows from the solar air heater to the evaporator then goes to ambient, Mode 4. The conventional solar air heater (the heat pump is omitted). For a conventional heat pump system thermal characteristics of R134a working fluid is better than the other two at the low-temperature applications such as space heating. Serial solar assisted heat pump modes, Mode 2 and Mode 3, shows better performance than the conventional types of operation. Mode 2 can be used a wide range of air mass flow rates while Mode 3 is limited to low rates. The performance of the Mode 2 is also higher than that of Mode 3 when R22 and R134a refrigerants are used. It is also shown that R134a yields a higher COP than R404a by more than 23% in the full range.

Kuang et al. [16] made an experimental research to measure the thermal performances os the overall system and its major components such as collector efficiency, energy consumption and COP of the heat pump during 2000-2001 heating season in China. A solar heating system with a water source heat pump was investigated. Because the water source hjeat pump allowed the solar collector to run at a lower temperature, sometimes even lower than the ambient temperature, the collector heat loss to the surroundings was greatly reduced and sometimes the colloctor even obtained heat from ambient air by convection on its cover. In their experimental study, since the evaporating temperature was relatively stable, the heat pump COP was determined mainly dependent on the condensing temperature. In this situation, COP will increase wit drop of the condensing temperature as a result of thermodynamical relations.

Chaturvedi et al. [17] used a direct expansion solar assisted heat pump in their setup. The compressor of the heat pump had variable frequency and operated at different speeds. Experiments showed that after reaching steady state condition, if the frequency was reduced, the thermal capasity rate reduced, but the COP increased due to a proportionately higher reduction in compressor power input. The reason for this improvement in COP is that the reduction in the mass of the refrigerant in the collector leads to higher collector temperature. A significant increase in the COP of the system can be achieved by modulating the compressor capacity with respect to the season.

Hawlader et al. [18] also used a variable speed compressor to obtain proper matching between the evaporator which is also the collector load and compressor capacity. Results showed that when water temperature in the condenser increased, the corresponding COP and collector efficiency values decreased. Results also showed that the performance of the system is influenced significantly by collector area, compressor speed and solar radiation. If the speed of the compressor increases, the collector/evaporator efficiency increases because there is reduction in evaporating temperature in the collector which results in a reduction of heat loss to the surroundings from the collector. On the other hand, COP value decreases with increasing compressor speeds since higher moss flow rates of the refrigerant in the collector/evaporator lead to higher compressor works. This mismatch was overcome by using the variable speed compressor. For a particular collector area, if solar radiation increases, COP increases since the evaporation temperature increases and causes to a reduction in compressor work. Finally, if difference between the ambient temperature and the fluid temperature in the collector increases, collector efficiency decreases due to increasing heat loss to the surroundings.

Badescu [19] placed PV cells and solar air heater on the south oriented part of the roof of a building. The PV array delivered electric power for necessities of this building whics acts as a laboratory. The compressor of the heat pump also reveived electricity from the PV cells. An important design parameter was the thermal energy storage unit length L. COP increased when temperature difference between the condenser and vaporizer decreased by decreasing length of the storage tank unit. On the other hand, monthly thermal energy stored by the storage tank and monthly energy necessity for the compressor were increased by in increasing storage tank unit length. The maximum heat flux was extracted from the storage unit during the morning.

Huang and Lee [20] tested a long-term reliability of an integral type solar assisted heat pump water heater. He designed a heat exchanger/condenser unit with a thermosyphon loop for reducing cost and obtaining high reliability. The waterside of the heat exchanger absorbed the heat from the condenser of a Rankine cycle by a

natural-convection flow in the thermosyphon loop. Experiments indicated that low daily hot water load made an increase in the daily initial water temperature in the tank and decrease the COP as well as electricity consumption. ISAHP must be designed to properly meet the daily hot water load reguirement. Oversized designs in hot water supply capasity cause a drop in the energy efficiency significantly. The study verifies that ISAHP has a high reliability and very low energy consumption even under long-term outdoors operating conditions such as wind and ambient temperature.

Göktun and Er [21] tried to determine the optimum performance of the systems by concerning solar asisted combined irreversible absorption-vapor compression cycle for air-conditioning and heat pump. They took into consideration the effect of internal irreversibilities on the performance of the hybrid system. Analysis of the system showed that the cycle irreversibility parameter has a strong effect on the maximum COP of the overal system for a given value of the operating parameter γ which is formulated by $\gamma=(\tau\alpha).\rho.I/(U.T_A)$ where $(\tau\alpha)$ is the transmittance-absorptance product, ρ is the concentration ratio, I is the average global solar irradition, U is the overall heat transfer coefficient and T_A is the ambient temperature. Maximum overal heating and cooling COPs increase when irreversibilitly parameter increases because if the parameter approachs to 1, the system approachs to reversible case. The parameter γ, on the other hand, should be larger than about 1 for optimum performance.

Yumrutaş and Kaşka [22] investigated the effects of climatic conditions and operating parameters on the performance of the system. The system became a model for residental heating applications in the southern region of the Turkey which has mild climatic conditions and high level of solar radiation with plenty of clear days. They concluded that heat pumps and solar systems are well-matched systems because of high COP and reasonable collector efficiency values.

CHAPTER 3

THEORETICAL STUDY AND DESIGN CONDITIONS

In this chapter, the coefficient of performance for the heat pump system and the collector efficiency for the solar heating system are determined theoretically. In addition, optimum tank configuration is designated by using the energy balance equations between the collector and heat pump systems.

3.1 Estimation of the Solar Energy Data

It is necessary to calculate the solar radiation received by the solar collectors in order to determine the useful solar energy gain.

3.1.1 Main Parameters for Solar Gain

Latitude of the location (L=39.95 for Ankara) and declination angle are the main parameters for starting to the estimation of solar radiation. Latitude is the angular distance between the location and the imaginary equator line (positive for north hemisphere). Declination is the angle made by the line joining the centers of the sun and the earth with its projection on the equatorial plane and is calculated by [23]:

$$D = 23.45 \cdot \sin\left[360 \cdot \frac{(284+n)}{365}\right] \tag{3.1}$$

where n is the number of day in a year ($1 \leq n \leq 365$).

Hour angle (w) is another main angle and is the angle between the longitude of the considered location and the line connecting the center of the earth. The hour angle is

zero at local solar noon and changes by 15^o per hour (360/24) for earlier or later than noon. It has positive sign for afternoon hours, negative sign for morning hours.

Zenith angle (Z) is the angle between the sun's rays and vertical line to the horizontal plane and can be derived from three angles before as follows:

$$Z = \arccos(\cos L \cdot \cos D \cdot \cos w + \sin L \cdot \sin D) \tag{3.2}$$

The solar altitude angle (α) is the angle between the sun's rays and the horizontal projection of the sun's rays. So that, it is complementary angle with the zenith angle and can be expressed by:

$$\alpha = \frac{\pi}{2} - Z \tag{3.3}$$

The solar azimuth angle ($\varnothing$) is the angle of sun's rays measured in the horizontal plane from due south, westward being designated as positive for the northern hemisphere. It can be found by the following relation [24]:

$$\varnothing = \arcsin(\cos D \cdot \frac{\sin w}{\cos \alpha}) \tag{3.4}$$

The surface azimuth angle (γ) is the deviation of the projection on a horizontal plane of the normal to the surface from the local meridian, with zero due south, east negative, west positive ($-180^0 \leq \gamma \leq 180^0$). It is very reasonable to fix the collector surface due south to receive more radiation for long-term studies.

Solar collectors are placed in a tilt angle (T) from the horizontal plane to obtain the maximum solar potential. The tilt angle (slope) can be taken as monthly average value considering the season and the location because it is an expensive method to track the sun at any moment.

The calculation of the length of a day is necessary to determine the solar gain for hourly basis. It enables to know the sunrise and sunset hours for a particular day. Hour angle at sunset can be determined by:

$$w_s = \arccos(-\tan L \cdot \tan D) \tag{3.5}$$

and the length of the day (the number of daylight hours) is expressed as follows:

$$N = \frac{2}{15} \cdot w_s \tag{3.6}$$

3.1.2 Hourly Total Radiation on a Horizontal Surface

3.1.2.1 Extraterrestrial Radiation

The radiation that would be received in the absence of the atmosphere is called extraterrestrial radiation. It can be calculated between hour angles w_1 and w_2 as follows in J/m^2 [23]:

$$I_0 = \frac{12 \cdot 3600}{\pi} \cdot G_{sc} \cdot (1 + 0.033 \cdot \cos\frac{360 \cdot n}{365})$$

$$\times \left[\cos L \cdot \cos D \cdot (\sin w_2 - \sin w_1) + \frac{\pi \cdot (w_2 - w_1)}{180} \cdot \sin L \cdot \sin D \right] \tag{3.7}$$

where G_{sc} is solar constant in the value of 1367 W/m^2.

3.1.2.2 Estimation of Hourly Radiation from Daily Data

The calculation of the performance for a system in short-time bases makes necessary the use of daily solar radiation data. Thus, daily radiation or monthly average daily radiation by meteorological data can be used to calculate the hourly radiation.

In this theoretical study, monthly average daily solar radiation data for Ankara were used. Statistical studies have lead to r_t ratio, the ratio of hourly total to daily total radiation, and it is expressed by Collares-Pereira and Rabl [23]:

$$r_t = \frac{I}{H} = \frac{\pi}{24}(a + b \cdot \cos w) \cdot \frac{\cos w - \cos w_s}{\sin w_s - \frac{\pi \cdot w_s}{180} \cdot \cos w_s} \tag{3.8}$$

where w is the hour angle in degrees for the time in question.

The coefficients a and b are given by:

$$a = 0.409 + 0.5016 \cdot \sin(w_s - 60) \tag{3.9}$$

$$b = 0.6609 + 0.4767 \cdot \sin(w_s - 60) \tag{3.10}$$

3.1.2.3 Beam and Diffuse Component of Hourly Radiation

The fraction hourly diffuse radiation on a horizontal surface can be expressed by the Erbs correlation [23]:

$$\frac{I_d}{I} = \begin{cases} 1.0 - 0.09k_T & \text{for } k_T \le 0.22 \\ (0.9511 - 0.1604 \cdot k_T + 4.388 \cdot {k_T}^2 & \\ \quad -16.638 \cdot {k_T}^3 + 12.336 \cdot {k_T}^4) & \text{for } 0.22 < k_T \le 0.80 \\ 0.165 & \text{for } k_T > 0.80 \end{cases} \tag{3.11}$$

where k_T is the hourly clearness index and is expressed as a function of the extraterrestrial radiation as follows:

$$k_T = \frac{I}{I_0} \tag{3.12}$$

Consequently, hourly beam radiation on a horizontal plane can be written by using the hourly diffuse and the total radiation data as follows:

$$I_b = I - I_d \tag{3.13}$$

3.1.3 Hourly Total Radiation on a Tilted Surface

One of the most important factors to gain the maximum available solar radiation for a certain season or month is the tilt angle. There are several suggestions on the collector tilt angle as dependent on the latitude of the place where the collector is located. Duffie and Beckman make a seasonal suggestion; for summer period $T = L$ -10 , for winter period $T = L + 10$ and for whole year period $T = L$.

It is necessary to define the ratio of total radiation on the tilted surface to that on the horizontal surface R :

$$R = \frac{\text{Total radiation on a tilted surface}}{\text{Total radiation on a horizontal surface}} = \frac{I_T}{I} \tag{3.14}$$

and for beam radiation:

$$R_b = \frac{\text{Beam radiation on a tilted surface}}{\text{Beam radiation on a horizontal surface}} \tag{3.15}$$

The ratio of beam radiation on a tilted surface to that on a horizontal surface can also be determined by the other equation for the northern hemisphere [23]:

$$R_b = \frac{\cos(L-T)\cdot\cos D\cdot\cos w + \sin(L-T)\cdot\sin D}{\cos L\cdot\cos D\cdot\cos w + \sin L\cdot\sin D} \tag{3.16}$$

A tilted surface also receives solar radiation reflected from the ground and other surroundings. By using a simple isotropic diffuse model, that is the assumption

of that the combination of diffuse and ground reflected radiation is isotropic, total solar radiation on a tilted surface can be calculated by Liu and Jordan [23]:

$$I_T = I_b \cdot R_b + I_d \cdot (\frac{1+\cos T}{2}) + I \cdot \rho_g \cdot (\frac{1-\cos T}{2}) \qquad (3.17)$$

where $(1+\cos T)/2$ term is the view factor to the sky, $(1-\cos T)/2$ term is the view factor to ground for tilted surface and ρ_g is the diffuse reflectance (or ground albedo) for the surroundings.

Optimum tilt angle can be calculated by the derivation of the total solar radiation on a tilted surface with respect to the tilt angle.

3.1.4 Mathematical Model for Hourly Total Solar Radiation

A mathematical simulation model by Mathcad is developed to estimate the hourly total radiation by using the general equations and necessary meteorological data for constant latitude and for all days of the year. The model can optionally calculate the beam and the diffuse radiations.

3.2 The Calculations of an Evacuated Tubular Heat-Pipe Solar Collector

Solar collector is the most important component for a solar system to convert the solar radiation to the heat form of energy. An evacuated-tube heat-pipe solar collector was used in this study. These collectors have the advantages of higher performance and higher temperature since heat losses by convection can be eliminated because of the vacuum inside the glass tube. Furthermore, heat pipes make thermal diode effect so that heat transfer is always in one direction, from absorber to the manifold, and never the reverse. In this study, Vitosol-300 H20 type vacuum tube collector based on the heat pipe principle produced by Viessmann Company were used (Figure 3.1).

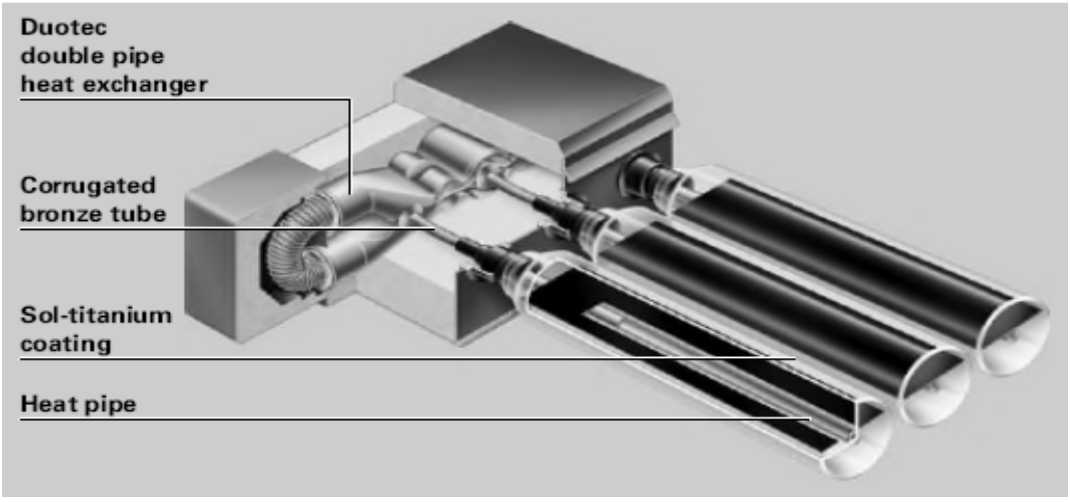

Figure 3.1 Viessmann Vitosol-300 H20 type vacuum tube heat-pipe solar collector.

Table 3.1 contains the specification of the solar collector and Figure 3.2 shows the main components of the collector system. A heat pipe filled with an evaporator liquid is arranged on the absorber. The heat pipe is connected to the condenser via a flexible coupling. The condenser is mounted in a Duotec double pipe heat exchanger. This involves a so-called “dry connection”, i.e. the tubes can be rotated or replaced even when the installation is filled and under pressure.

Heat is transferred from the absorber to the heat pipe. This heat transfer evaporates the liquid. The vapor then rises to the condenser of the collector. The heat is transferred to the passing heat transfer medium (water in the loop) by the double-pipe heat exchanger containing the condenser (manifold); this causes the vapor to condense. The condensate returns into the heat pipe by gravity and the process is repeated [25].

Deviations from the south direction can be compensated by axial rotation of the vacuum tubes.

The collector temperature sensor is installed inside a sensor mounting on the flow pipe in the collector connection housing [25].

Table 3.1 Specifications of Viessmann Solar Panel Vitosol 300 H20.

Number of pipes		20
Gross area	m^2	2.94
Absorber surface area	m^2	2
Aperture area	m^2	2.14
Dimensions Width Height Depth	 mm mm mm	 1450 2024 138
Optical efficiency[*1]	%	82.5
Heat loss factor k_1[*1] k_2[*1]	$W/(m^2.K)$ $W/(m^2.K^2)$	1.19 0.009
Weight	kg	45
Liquid content (heat transfer medium)	litres	1.2
Permissible operating pressure[*2]	bar	6
Max. idle temperature	^0C	150
Connection	ø mm	22
Space requirement for flat roof installations	m^2	approx. 1.3

[*1] *Relative to the absorber surface area.*

[*2] *The collectors must be pressurised in cold, sealed systems with at least 1.5 bar.*

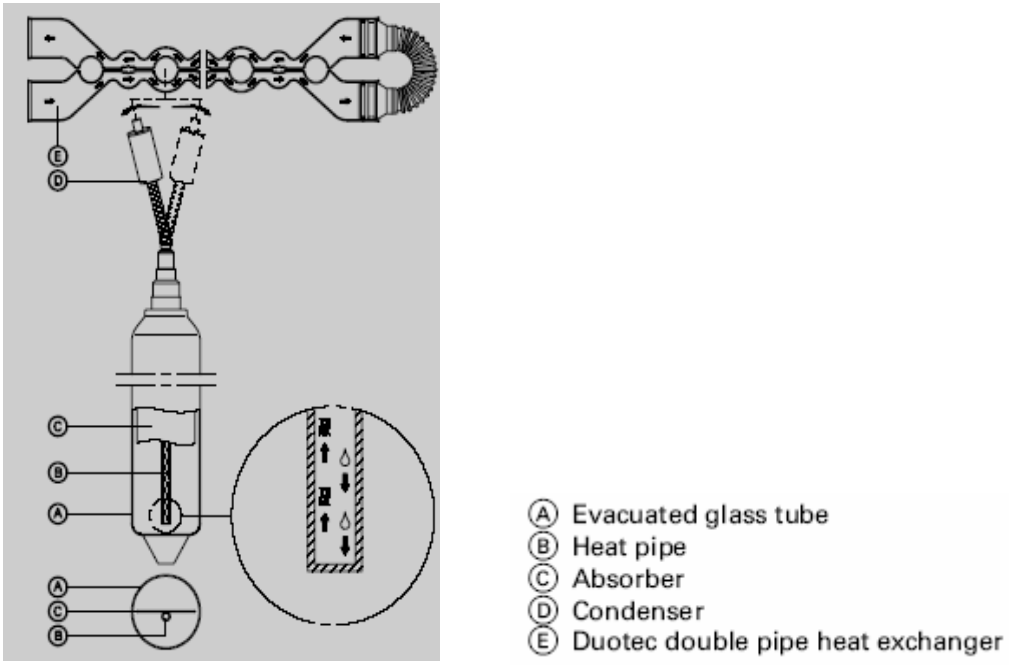

Figure 3.2 Main components of the evacuated heat-pipe solar collector.

3.2.1 Performance Analysis of the Evacuated-Tube Heat-Pipe Solar Collector

Simple energy balance procedure can be applied to find the steady state performance of an evacuated-tube heat-pipe collector. Figure 3.3 shows the distribution of the absorbed radiation into the useful energy gain and thermal losses by using electrical analogy [26].

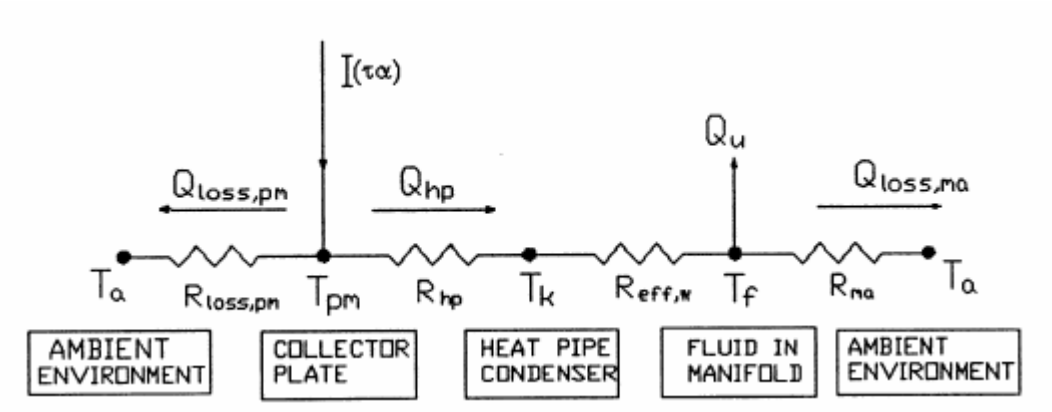

Figure 3.3 The equivalent thermal circuit for a heat-pipe solar collector.

The incident solar radiation that falls on an absorber of unit area is given by the product of solar irradiance (I) and transmittance-absorptance coefficient ($\tau\alpha$). The latter terms represent the optical loss when the radiation passes through the collector glass cover. Then, a part of this absorbed radiation by the absorber is dissipated to the surroundings by heat losses. These losses can be defined here as the difference between the absorber plate temperature T_{pm} and the ambient temperature T_a divided by the thermal resistance $R_{loss,pm}$. A major part of the incident energy is transferred to the heat pipe of the collector that rejects the energy to the circulating coolant (water here) at the condenser. This energy is then extracted by the circulating fluid that gives the useful effect, Q_u. Part of Q_u is also lost to the ambient through heat leaks from the manifold as shown by the resistance term, R_{ma}. They should be emphasized that all thermal resistances are normalized with respect to the manifold area A_{ma} and convective losses are assumed negligible [26].

The balance of heat transfer rates of evacuated-tube heat-pipe solar collectors can be written from Figure 3.3 as follows [26]:

$$q_{in} = q_{loss,rad} + q_{hp} = q_{loss,rad} + q_u + q_{loss,ma} \tag{3.18}$$

This equation can be written in terms of incident solar radiation, thermal resistances and temperatures by [26]:

$$\frac{I \cdot (\tau\alpha) \cdot A_c}{A_{ma}} = \frac{T_{pm} - T_a}{R_{rad}} + q_u + \frac{T_f - T_a}{R_{ma}} \tag{3.19}$$

where $(\tau\alpha)$ is transmittance-absorptance product and A_c is collector area. Thermal resistance for heat loss by radiation between the absorber and the ambient is expressed by [26]:

$$R_{rad} = \frac{(T_{pm} - T_a) \cdot A_{ma}}{\varepsilon \cdot \sigma \cdot ({T_{pm}}^4 - {T_a}^4) \cdot A_c} \tag{3.20}$$

Replacing T_{pm}-T_a by q_{hp}, R_{hp} and $R_{eff,w}$ and defining $R_{hr}=R_{hp}/R_{rad}$ as well as $R_{er}=R_{eff,w}/R_{rad}$ as follows [26]:

$$\frac{T_{pm} - T_a}{R_{rad}} = \frac{T_f - T_a}{R_t} = \frac{(T_f - T_a) \cdot (R_{hr} + R_{er} + 1)}{R_{rad} \cdot (R_{hr} + R_{er})} \tag{3.21}$$

where

$$\frac{1}{R_t} = \frac{1}{R_{rad}} + \frac{1}{R_{hp} + R_{eff,w}} = \frac{R_{hr} + R_{er} + 1}{R_{rad} \cdot (R_{hr} + R_{er})} \tag{3.22}$$

Equation (3.19) becomes a useful equation for the energy from the collector in the form :

$$q_u = \frac{I \cdot (\tau\alpha) \cdot A_c}{A_{ma}} - \frac{T_f - T_a}{(R_{hr} + R_{er})}\left[\frac{1}{R_{rad}} \cdot (R_{hr} + R_{er} + 1) + \frac{1}{R_{ma}} \cdot (R_{hr} + R_{er})\right] \quad (3.23)$$

Thermal resistance and heat transfer coefficient of heat pipe are given by [26]:

$$R_{hp} = \frac{A_{ma}}{h_{hp} \cdot A_{cond}} \quad \text{and} \quad h_{hp} = 0.555\left[\frac{\rho^2 \cdot g \cdot k^3 \cdot h_{fg}}{\mu \cdot D_{cond} \cdot (T_{pm} - T_k)}\right]^{1/4} \quad (3.24)$$

and thermal resistance of condenser is given by [26]:

$$R_{eff,w} = R_w + R_f \text{, where } R_w = \frac{t}{k} \text{ and } R_f = \frac{1}{h_f} \quad (3.25)$$

where t is the thickness of condenser wall in m and $Nu = 0.023 \cdot Pr^{0.4} \cdot Re^{0.8}$ for h_f. Thermal resistance of manifold can be found by [26]:

$$R_{ma} = \frac{A_{ma}}{U_{ma} \cdot A_{ma,loss}} \quad (3.26)$$

The useful heat gain in a collector may be expressed in terms of solar radiation, the heat loss coefficient, the temperatures of coolant and ambient and the collector efficiency factor as follows [26]:

$$q_u = \frac{F' \cdot A_c}{A_{ma}}\left[I \cdot (\tau\alpha) - U_L \cdot (T_f - T_a)\right] \quad (3.27)$$

where the collector efficiency factor is given by [26]:

$$F' = \frac{1}{R_{hr} + R_{er} + 1} \quad (3.28)$$

and the overall heat loss coefficient is given by [26]:

$$U_L = \frac{A_{ma}}{R_{rad} \cdot A_c} + \frac{A_{ma}}{R_{ma} \cdot A_c \cdot F'} \tag{3.29}$$

The collector heat removal factor (F') can be introduced to simplify the heat gain expression by integrating equation (3.27) with respect to the appropriate boundary conditions ($T_{z=0}=T_i$ *and* $T_{z=L}=T_o$) and resulting equation becomes as follows [26]:

$$Q_u = A_c \cdot F_R \cdot \left[S - U_L \cdot (T_i - T_a) \right] \tag{3.30}$$

where $S = I \cdot (\tau\alpha)$ is the absorbed radiation and the heat removal factor (F_R) is equivalent to the effectiveness of a heat exchanger and can be written by [26]:

$$F_R = \frac{m \cdot c_p \cdot (T_o - T_i)}{A_c \cdot \left[S - U_L \cdot (T_i - T_a) \right]} \tag{3.31}$$

The instantaneous collector efficiency at steady state, defined as the ratio of the useful energy gain to the incident radiation over a finite interval, is simply given by:

$$\eta_c = \frac{Q_u}{A_c \cdot I} = \frac{F_R \cdot \left[I \cdot (\tau\alpha) - U_L \cdot (T_i - T_a) \right]}{I} \tag{3.32}$$

A number of tests from the producer company yield to the following thermal performance equations (look at Table 3.1):

Linear fit: $$\eta = 0.825 - 1.19 \cdot \frac{T_i - T_a}{I} \tag{3.33}$$

Second order fit: $$\eta = 0.825 - 1.19 \cdot \frac{T_i - T_a}{I} - 0.009 \cdot \left(\frac{T_i - T_a}{I} \right)^2 \tag{3.34}$$

T_i is the inlet temperature of the fluid. For I =800 W/m^2 constant solar irradiance and T_a=15 ^{o}C ambient temperature, the collector efficiency curve based on the second order fit can be seen from Figure 3.4. In linear fit, first constant (0.825) indicates the intercept (maximum value) of the efficiency and second constant (1.19) indicates the slope of the collector efficiency.

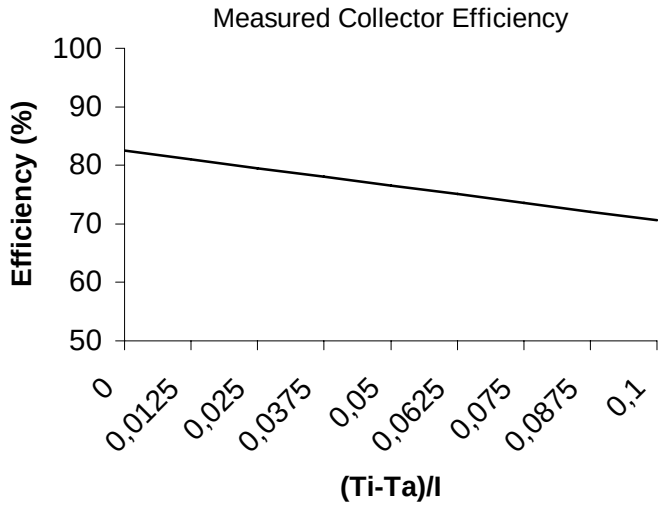

Figure 3.4 Evacuated tube collector efficiency curve.

3.3 Storage Tank Unit

It is necessary to use a storage system for thermal applications in order to solve the problem of the mismatch between the thermal loads of the building and intermittent and unpredictable rates of the solar radiation. The major components of a solar assisted heat pump with storage are the solar collector, the storage unit, the heat pump as a conversion device, auxiliary energy supplies and control system. The expected available solar radiation, necessary thermal loads for the thermal applications, the need for auxiliary energy, and economic analysis between the solar system and auxiliary energy supply are the factors in determination of the capacity of the storage system.

Water is the ideal material to store heat because energy is transferred to or from the storage unit by transport of the storage medium itself and thus temperature drop between the storage medium and transport fluid can be eliminated. Water is also inexpensive, nontoxic and widely available. Furthermore, this type of storage is sensible heat storage unless the phase of the water changes into vapor phase, namely below 100 ^{0}C. So, the amount of energy stored can be expressed by temperature difference as follows:

$$E = m \cdot \int_{T_1}^{T_2} c_p \cdot dT \tag{3.35}$$

where T_1 and T_2 represent the lower and upper temperature levels between which the storage operates.

3.3.1 Heat Losses from the Storage Tank

The geometry of the storage tank is cylindrical and heat losses of the tank consist of side loss, top and bottom losses:

$$Q_{\text{tank}} = Q_{side} + Q_{top} + Q_{bottom} \tag{3.36}$$

Figure 3.5 shows the temperature distribution for the cylindrical wall.

Heat transfer rate from the side to the surroundings can be calculated as follows:

$$q_r = \frac{T_{\infty,1} - T_{\infty,3}}{\frac{1}{2 \cdot \pi \cdot r_1 \cdot L \cdot h_1} + \frac{In(r_2 / r_1)}{2 \cdot \pi \cdot k_{sheet} \cdot L} + \frac{In(r_3 / r_2)}{2 \cdot \pi \cdot k_{ins} \cdot L} + \frac{1}{2 \cdot \pi \cdot r_3 \cdot L \cdot h_3}} \tag{3.37}$$

It can be assumed that the temperature of the tank inside the wall is same as that of the water in the tank. So, inside convective heat transfer coefficient can be neglected. In this case, total thermal resistance may be expressed as:

$$R_t = \frac{1}{U_1 \cdot A_1} = \frac{In(r_2 / r_1)}{2 \cdot \pi \cdot k_{sheet} \cdot L} + \frac{In(r_3 / r_2)}{2 \cdot \pi \cdot k_{ins} \cdot L} + \frac{1}{2 \cdot \pi \cdot r_3 \cdot L \cdot h_3} \tag{3.38}$$

Note that:

$$U_1 \cdot A_1 = U_2 \cdot A_2 = U_3 \cdot A_3 = \frac{1}{R_t} \tag{3.39}$$

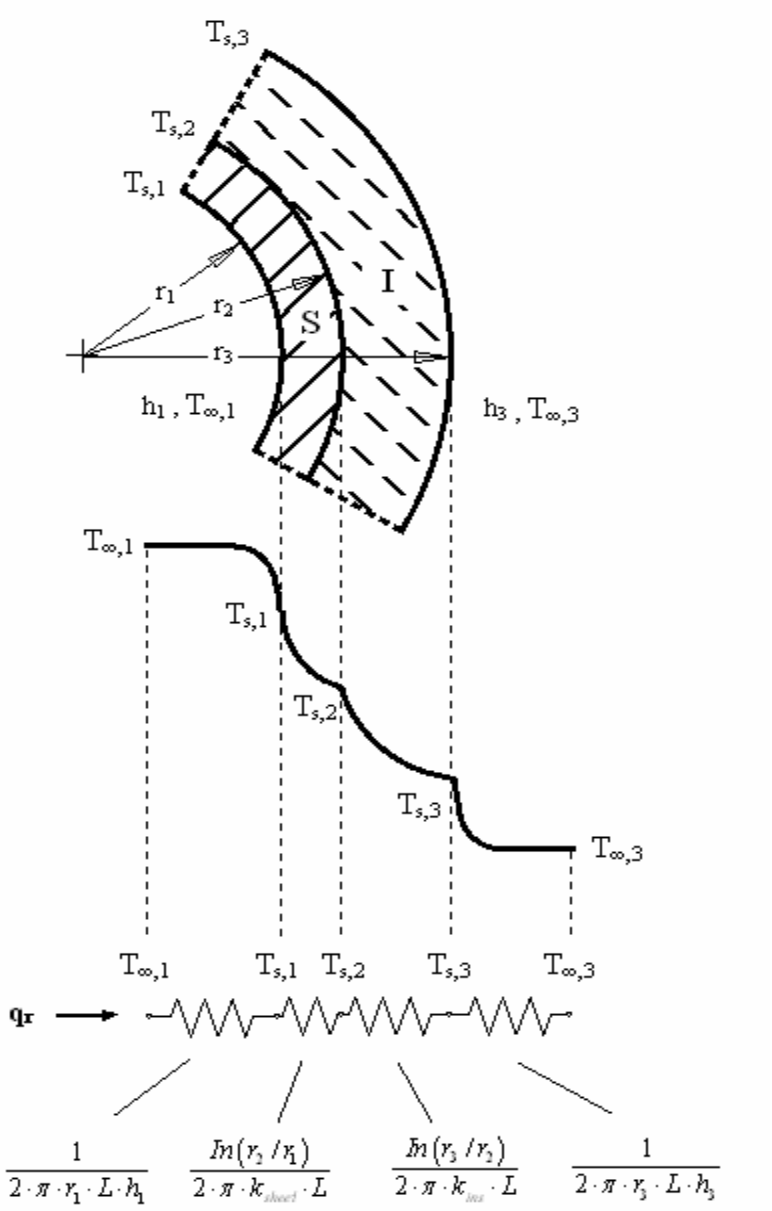

Figure 3.5 Temperature distributions for a cylindrical wall.

Figure 3.6 shows the dimensions of the tank:

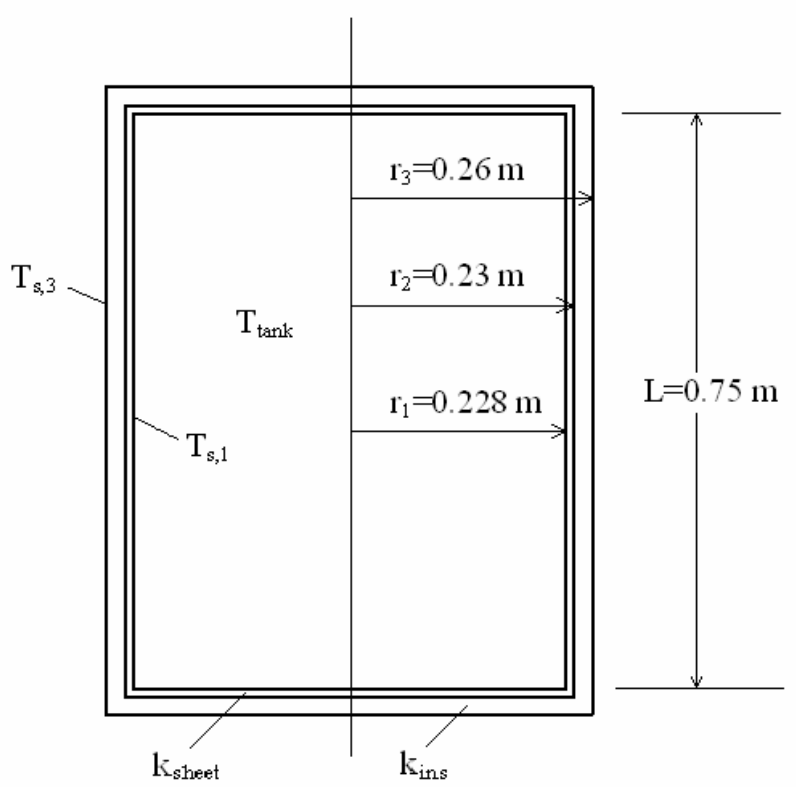

Figure 3.6 The storage tank geometry.

Outer heat transfer coefficient can be found by free convection correlations since storage tank has been placed inside the room and has not been affected from wind speeds. The correlations for a vertical plate may also be used for a vertical cylinder since the following condition is satisfied [27, 28]:

$$\frac{D}{L} \geq \frac{35}{Gr^{1/4}} \tag{3.40}$$

where D and L are the diameter and the height of the cylinder, respectively. The Grashof number (Gr) is dependent on outer surface and ambient temperatures as follows [27]:

$$Gr_L = \frac{g \cdot \beta \cdot (T_s - T_\infty) \cdot L^3}{v^2} \tag{3.41}$$

g is the gravitational acceleration (m/s^2), β is the thermal expansion coefficient (1/K), L is the height of the tank (m), v is the kinematic viscosity (m^2/s) and T_s and T_∞ are the temperatures of surface and ambient temperatures (K) respectively. Satisfying eqn. (3.39), outer convective heat transfer coefficient can be determined by:

$$\overline{h_o} = \frac{\overline{Nu}_L \cdot k}{L} \tag{3.42}$$

where k is the thermal conductivity (W/m.K) and Nusselt number ($\overline{Nu}_L$) is defined by:

$$\overline{Nu}_L = \left\{ 0.825 + \frac{0.387 \cdot Ra_L^{1/6}}{\left[1 + (0.492/Pr)^{9/16}\right]^{8/27}} \right\}^2 \tag{3.43}$$

Rayleigh number (Ra_L) and Prandtl number (Pr) are also temperature dependent.

Pr is read from the temperature-thermophysical properties tables for air at average temperature and Ra_L can be calculated from the equation below:

$$Ra_L = Gr_L \cdot Pr = \frac{g \cdot \beta \cdot (T_s - T_\infty) \cdot L^3}{v \cdot \alpha} \tag{3.44}$$

where α is the thermal diffusivity (m^2/s).

Corresponding temperatures can be selected in such a way that heat transfer coefficient has a maximum value of it in order to take the upper limit of heat loss into

consideration. Thus, the outer surface temperature can be taken 40 ^{0}C and the ambient temperature inside the room can be taken 20 ^{0}C. The other properties of air are looked for the average temperature $T_{ave} = (40+20)/2 = 30$ ^{0}C. Using this assumption and calculating necessary unknown parameters, a numerical solution can be obtained for the heat loss from sides. Calculation procedure is as follows:

$g = 9.81$ m/s^2 , $T_s = 40$ ^{0}C, $T_\infty = 20$ ^{0}C, $\beta = 1/T_{ave} = 1/303$ 1/K, $L = 0.75$ m

Air properties at 30 ^{0}C:

$k = 0.0267$ W/m.K, $v = 16\times10^{-6}$ m^2/s, $Pr = 0.701$

$$Gr_L = \frac{9.81\cdot 1/303\cdot(40-20)\cdot 0.75^3}{(16\times10^{-6})^2} = 1.07\times10^9$$

$$Ra_L = Gr_L \cdot Pr = 1.07\times10^9 \cdot 0.701 = 0.75\times10^9$$

$$\overline{Nu}_L = \left\{0.825 + \frac{0.387\cdot(0.75\times10^9)^{1/6}}{\left[1+(0.492/0.701)^{9/16}\right]^{8/27}}\right\}^2 = 112.24$$

$$\overline{h_o} = \frac{\overline{Nu}_L \cdot k}{L} = \frac{112.24\cdot 0.0267}{0.75} \cong 4 \text{ W/m}^2\text{.K}$$

$$(U\cdot A)_{side} = \frac{1}{\frac{In(0.23/0.228)}{2\cdot\pi\cdot14.2\cdot0.75} + \frac{In(0.26/0.23)}{2\cdot\pi\cdot0.04\cdot0.75} + \frac{1}{2\cdot\pi\cdot0.26\cdot0.75\cdot4}} = 1.17 \text{ W/K}$$

$k_{sheet} = 14.2$ W/m.K for stainless steel sheet and $k_{ins} = 0.04$ W/m.K for insulation material. After finding the side heat loss coefficient of the storage tank, top and bottom heat loss coefficients which are identical can be calculated by the equation below. Figure 3.7 shows the temperature distribution along the flat wall.

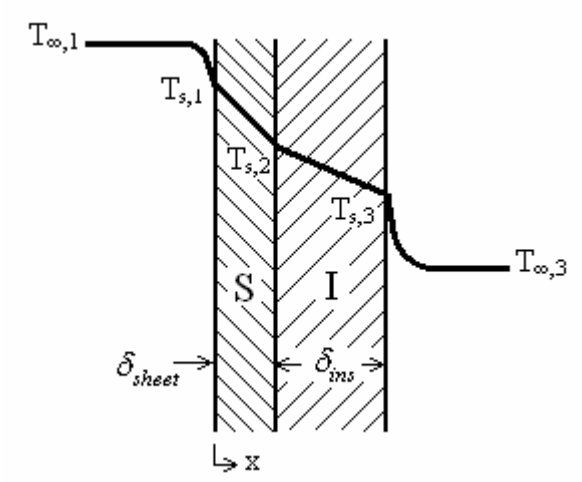

Figure 3.7 Temperature distribution for a flat wall.

$$U_{top} = U_{bottom} = \frac{1}{\frac{\delta_{sheet}}{k_{sheet}} + \frac{\delta_{ins}}{k_{ins}} + \frac{1}{\overline{h}_o}} \tag{3.45}$$

and

$$(U \cdot A)_{top+bottom} = 2 \cdot (U_{top} \cdot \pi \cdot r^2) \tag{3.46}$$

A numerical solution can be obtained substituting the known values into the last two equations above as follows:

$$U_{top} = \frac{1}{\frac{0.002}{14.2} + \frac{0.03}{0.04} + \frac{1}{4}} \cong 1 \text{ W/m}^2\text{.K}$$

$$(U \cdot A)_{top+bottom} = 2 \cdot (1 \cdot \pi \cdot 0.23^2) = 0.33 \text{ W/K}$$

where $r = 0.23$ m. Finally, the total heat loss can be expressed by:

$$Q_{\text{tank}} = Q_{side} + Q_{top+bottom} = (U \cdot A)_{side} \cdot \Delta T + (U \cdot A)_{top+bottom} \cdot \Delta T = (1.17 + 0.33) \cdot \Delta T = 1.5 \cdot \Delta T$$

where ΔT is the temperature difference between the inside and the outside of the tank.

As a result, the heat loss from the tank to the surroundings can be neglected, since both the tank is already inside the room to be heated and, the heat loss has very small quantities relatively.

3.3.2 Heat Transfer Phenomena of the Evaporator inside the Tank

The original evaporator of the heat pump system was disbanded from the other components and a new helical coil evaporator was made from 3/8" copper tubes. This helical coil was located in the storage tank.

The heat transfer rate from the hot water in the tank to the refrigerant in the evaporator is one of the important parameters in the calculation of the COP of the heat pump system. The heat transfer rate at the evaporator can be calculated in W by following equation [28]:

$$Q_L = \frac{T_w - T_e}{\frac{1}{h_i \cdot A_i} + \frac{\ln\left(\frac{r_o}{r_i}\right)}{2 \cdot \pi \cdot k_t \cdot L} + \frac{1}{h_o \cdot A_o}} \tag{3.47}$$

where

T_w = Temperature of the water in the tank (^oC)

T_e = Evaporation temperature of the refrigerant (^oC)

h_i = Convection heat transfer coefficient inside the evaporator coil (W/m^2K)

h_o = Convection heat transfer coefficient outside of the evaporator coil (W/m^2K)

k_t = Thermal conductivity of the copper tube (W/mK)

L = Coil length (m)

r_o, r_i = Outer and inner radius of the copper tube respectively (m)

A_o, A_i = $\pi.D_o.L$, $\pi.D_i.L$ =Outer and inner surface area of the tube respectively (m^2)

Convective heat transfer coefficient inside the coil can be determined by boiling heat transfer correlation [29]:

$$h_i = 0.00417 \cdot q_{\max}{}^{0.7} \cdot P_{crit}{}^{0.69} \cdot F_p \tag{3.48}$$

$$F_p = 1.8 \cdot P_r^{0.17} + 4 \cdot P_r^{1.2} + 10 \cdot P_r^{10} \tag{3.49}$$

where

q_{max} = Max. heat flux at the evaporator (W/m^2)

P_{crit} = Critical pressure of the refrigerant (4619 kPa for R407C)

P_r=P/P_{crit} = Reduced pressure of the refrigerant at max. heat flux (nondimensional)

Nusselt number for finding outer convection heat transfer coefficient can be obtained by applying natural convection correlation due to very low mass flow rate of the water in the tank [27, 30]:

$$Nu = C \cdot Ra^m \tag{3.50}$$

where Rayleigh number can be found as follows:

$$Ra = \frac{9.81 \cdot \beta \cdot \left(T_w - T_e\right) \cdot D_o{}^3 \cdot Pr}{v^2} \tag{3.51}$$

β =$1/T_f$ = Thermal expansion coefficient at T_f (1/K) (T_f : average temperature)

D_o = Outer diameter of the tube (m)

Pr = Prandtl number of the water at T_f (nondimensional)

v = Kinematic viscosity of the water at T_f (m^2/s)

C and m constants of eqn. (3.50) can be determined from the following table according to Ra number:

Table 3.2 C and m constants for eqn. (3.50).

Ra	C	m
$10^{-2} - 10^{2}$	1.02	0.148
$10^{2} - 10^{4}$	0.85	0.188
$10^{4} - 10^{7}$	0.48	0.25
$10^{7} - 10^{12}$	0.125	0.333

Knowing the Nusselt number, outer heat transfer coefficient can be calculated by:

$$h_o = \frac{Nu \cdot k}{D_o} \tag{3.52}$$

where k is the thermal conductivity of the water at T_f in W/mK.

3.4 Heat Transfer Rate at the Condenser

The other important parameter for a heat pump is the heat transfer rate at the condensation. The condenser is a counter-flow heat exchanger and the air inside the room is sucked in this heat exchanger by means of a fan. The hot refrigerant passed through tubes leaves its energy to the air and heat transfer occurs between them.

The heat transfer rate at the condenser can be determined by following relation:

$$Q_H = \frac{\Delta T_{lm}}{\frac{1}{h_i \cdot A_i} + \frac{\ln(D_o / D_i)}{2 \cdot \pi \cdot k_t \cdot L} + \frac{1}{h_o \cdot A_o}} \tag{3.53}$$

where

h_i, h_o = Inner and outer convective heat transfer coefficients respectively (W/m^{2}K)

k_t = Thermal conductivity of the copper tube (W/mK)

L = Condenser tube length (m)

D_o, D_i = Outer and inner diameter of the copper tube respectively (m)

A_i = $\pi.D_i.L$ = Inner surface area of the tube (m^2)

A_o = Finned outer surface area of the tube (m^2)

Logarithmic mean temperature difference, ΔT_{lm} for counter flow can be calculated by [27]:

$$\Delta T_{lm} = \frac{(T_{h,i} - T_{c,o}) - (T_{h,o} - T_{c,i})}{\ln\left[\frac{(T_{h,i} - T_{c,o})}{(T_{h,o} - T_{c,i})}\right]} \tag{3.54}$$

$T_{h,i} = T_{h,o}$ = Constant condensing temperature of hot fluid (refrigerant) (^{o}C)

$T_{c,o}$, $T_{c,i}$ = Outlet and inlet temperature of cold fluid (air) (^{o}C)

The refrigerant side (inner) convective heat transfer coefficient is determined by the expression for condensation in horizontal tubes [30]:

$$h_i = 0.555 \cdot \left[\frac{9.81 \cdot \rho_f \cdot (\rho_f - \rho_g) \cdot h_{fg}{}' \cdot 10^3 \cdot \lambda_f{}^3}{\mu_f \cdot (T_s - T_w) \cdot D_i}\right]^{\frac{1}{4}} \tag{3.55}$$

where

T_s = saturation temperature (^{o}C)

T_w = wall temperature (^{o}C)

D_i = inner diameter of the tube (m)

ρ_f = saturated liquid density of the refrigerant at average temperature (kg/m^3)

ρ_g = saturated vapor density of the refrigerant at saturation temperature (kg/m^3)

λ_f = liquid thermal conductivity of the refrigerant at average temperature (W/mK)

μ_f = liquid dynamic viscosity of the refrigerant at average temperature (Pa.s)

Corrected latent heat $h_{fg}{}'$ is found by following equation:

$$h_{fg}{}' = h_{fg} + 0.375 \cdot c_{pf} \cdot (T_s - T_w) \tag{3.56}$$

where h_{fg} is latent heat of the refrigerant at saturation temperature in J/kg and c_{pf} is liquid specific heat of the refrigerant at average temperature in kJ/kgK.

The air side (outer) heat transfer coefficient can be determined by corresponding correlation by Grimison for airflow over a tube bank as follows [27]:

$$Nu_D = C \cdot (Re_{D,max})^m \tag{3.57}$$

$$Re_{D,max} = \frac{V_{max} \cdot D}{v} \tag{3.58}$$

where V_{max} is the maximum fluid velocity within the tube bank in m/s. C and m constants of eqn. (3.57) are dependent on the tube arrangement in the bank and can be taken from the tables in literature. Then outer heat transfer coefficient can be calculated as follows:

$$h_o = \frac{Nu_D \cdot k}{D} \tag{3.59}$$

3.5 Energy Balance on the Storage Tank

The solar system and the heat pump system are linked to each other in the storage tank. Water is commonly used as a heat storage medium because of its low cost and high specific heat qualities.

An energy balance on the storage tank for unstratified uniform water temperature T_s can be written as follows [24]:

$$(m \cdot c_p)_s \cdot \frac{dT_s}{dt} = Q_u - Q_L - Q_{TL} \tag{3.60}$$

where

m = Mass of the water in the tank (kg)

c_p = Specific heat of the water (kJ/kgK)

Q_u = Rate of collected solar energy delivered to the storage tank (kW)

Q_L = Rate of heat absorbed by the evaporator (kW)

Q_{TL}= Rate of heat loss from the storage tank (kW)

The heating load supplied by solar energy via the evaporator can be expressed by:

$$Q_u = (m \cdot c_p)_s \cdot \Delta T \tag{3.61}$$

where m is mass flow rate of water in kg/s and ΔT is temperature drop of water in the tank. Heat loss from the tank can also be expressed by:

$$Q_{TL} = (U \cdot A)_s \cdot (T_s - T_a) \tag{3.62}$$

where $(U \cdot A)_s$ the loss coefficient of the storage tank and area product in kW/K and T_a is the ambient temperature. The loss coefficient was calculated numerically before from equations (3.38) and (3.39) and defined as overall value of 1.5 W/K. It was concluded that heat loss from the storage tank was negligible because of its small value in kW unit basis.

Equation (3.60) can be rewritten in finite-difference form for a period of time as follows:

$$(m \cdot c_p)_s \cdot \frac{T_s^{'} - T_s}{\Delta t} = Q_u - Q_L$$

or

$$T_s^{'} = T_s + \frac{\Delta t}{(m \cdot c_p)_s} \cdot (Q_u - Q_L) \tag{3.63}$$

where $T_s^{'}$ is the new temperature of the tank at the end of the period Δt in s.

CHAPTER 4

EXPERIMENTAL STUDY AND RESULTS

AE1AH16IW type air conditioner produced by General Electric Company was used for the experimental setup. Modifications were made on the air conditioner to connect it to the solar heating system. A solar assisted heat pump was constructed with these modifications. In this chapter, technical specifications and design parameters of the setup and measuring devices will be described.

4.1 Solar Assisted Heat Pump Test Facility

The air conditioner had two parts: indoor and outdoor units. The outdoor unit which was the evaporator of the heat pump was not needed in the experiments; therefore, it was not used. Instead, a heat exchanger was designed and fabricated to meet the evaporation load of the system. Compressor of the heat pump system was on the outdoor unit and was used without disbanding it from its original assembly. The indoor unit, i.e. condenser of the heat pump, was assembled on the wall inside the room. The storage tank linked the heat pump to solar energy system. The schematic representation of the components and some views of the test setup are given in Figure 4.1 and Figure 4.2 respectively.

The indoor unit is a heat exchanger that was used to heat the air inside the room. It acted as a condenser for the heat pump and increased the air temperature by using the higher refrigerant temperature. It had control panel and wiring cover on it. The expansion process was achieved by capillary tubes.

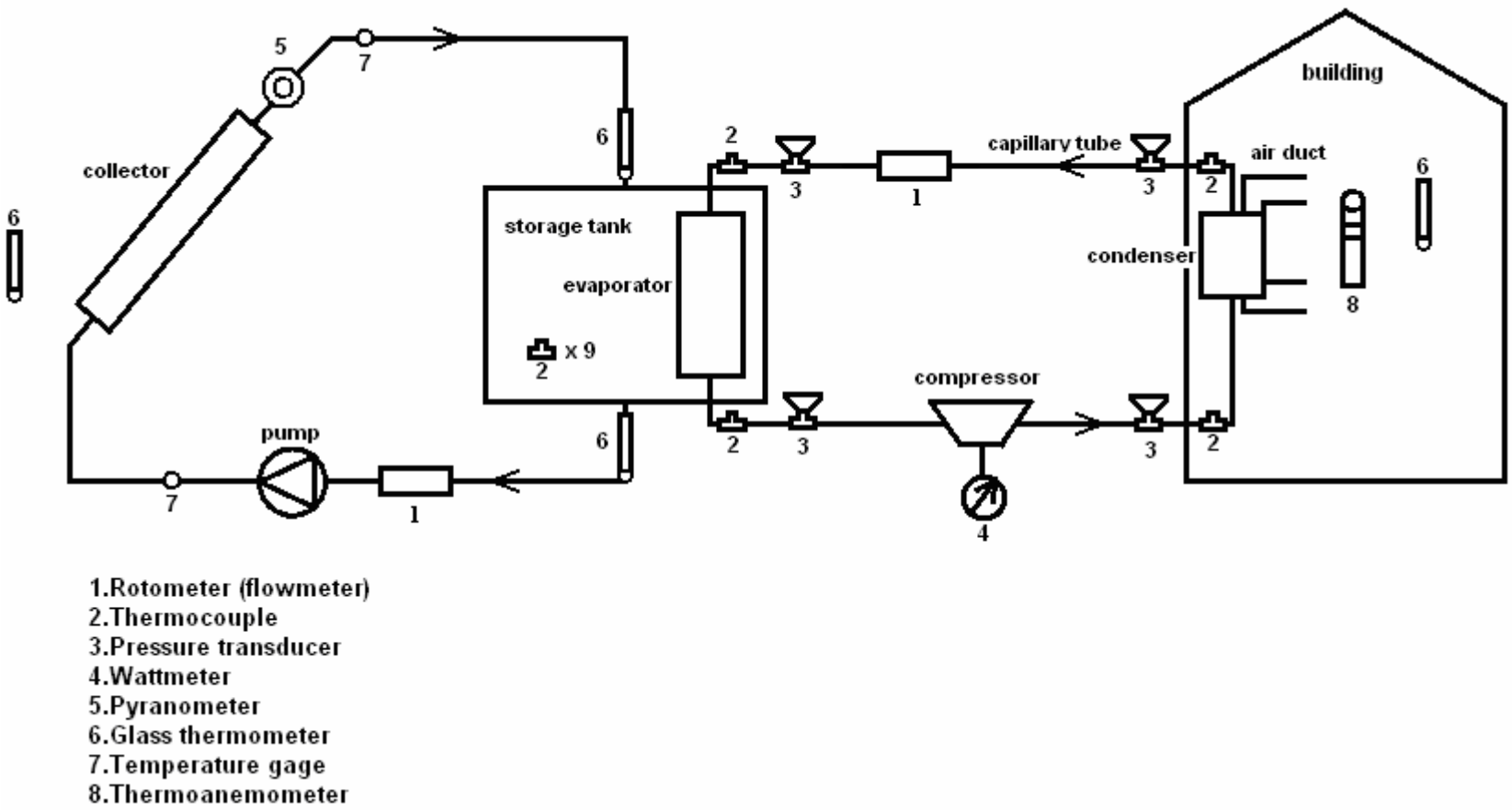

Figure 4.1 Shematic representation of the experimental setup.

Figure 4.2 Some views of the experimental setup.

The evaporator of the heat pump consisted of a helical coil. This coil was placed in the storage tank which acted as the heat source of the heat pump (Figure 4.3).

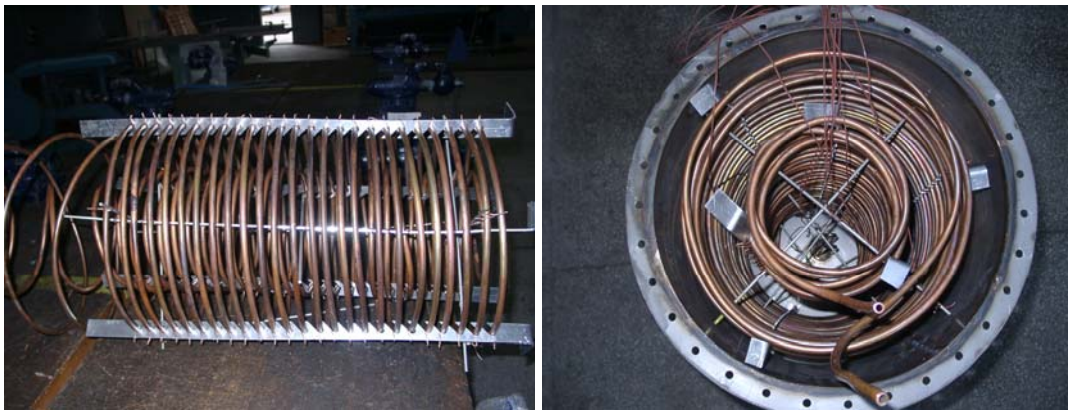

Figure 4.3 The evaporator coil and its arrangement into the storage tank.

Technical specifications of the air conditioner are listed in Table 4.1. It has the capability of doing both cooling and heating. A three-stage fan was involved on the indoor unit of the air conditioner to increase the heat transfer rate at the condenser.

Table 4.1 Technical specifications of the air conditioner

Type	AE1AH16IW (GE)
Rated voltage	230 V
Rated frequency	50 Hz
Rated current (Cooling)	7.9 A
Rated current (Heating)	7.9 A
Rated input (Cooling)	1750 W
Rated input (Heating)	1750 W
Cooling capacity	4500 W
Heating capacity	5200 W
Refrigerant	R407C

Connections of the main components of the heat pump to each other were made by copper piping. 3/8” and 1/2”-dia copper tubes were used at the inlet and the exit of the evaporator and the condenser. The evaporator was also made by 3/8” copper tube. R407C refrigerant that is the mixture of R32, R125 and R134a refrigerants was used in the heat pump system.

The evaporator of the heat pump was placed in 120-lt water storage tank and evaporation process of the heat pump cycle occurred in this hot water tank. The storage tank was linked to an evacuated tube solar collector and a closed system was formed. The pump of the collector system circulated hot water in this closed system.

Two thermostats were used in the storage tank, one of them was for preventing the formation of frost in the collector system and the other was for keeping the temperature of the tank constant when the solar gain was not sufficient. The thermostat was essential to be able to observe the performance characteristics of the system at desired temperatures. Besides, it was necessary not to drop the temperature in the tank below a certain value (5 ^{o}C) to avoid any damage in the collector system due to the formation of frost.

The system was checked for leakages by sending pressurized air to inside the pipes by using a different compressor.

4.2 Measuring Devices

Measuring devices were used to take data and calculate the energy transfer rates and make a performance analysis of the system. Measured properties were mainly temperatures and pressures at various locations, flow rates, consumption of electric power and solar energy gain. Measuring devices used can be seen in Figure 4.1.

4.2.1 Temperature Measurement

Most of the measurements made in this experimental study was the temperature. Four different devices were used to measure the temperature values at different locations. These can be listed as follows:

a. Thermocouples with a data acquisition system (datalogger)
b. Glass thermometers

c. Temperature gages

d. Thermoanemometer

It is necessary to know the temperatures of the refrigerants at the inlets and outlets of the components (the evaporator and the condenser) of a heat pump to determine the thermodynamic states and enthalpy values at those states to calculate the heat and work transfer rates. Therefore, four thermocouples were placed at the inlets and the outlets of the evaporator and the condenser of the heat pump. Nine thermocouples were also placed at different locations in the storage tank. One thermocouple was used to measure the inside room temperature and one thermocouple was used to measure the ambient temperature.

Two thermocouples were placed at the inlet and the outlet of a fan coil unit which was used to reject excess heat from the system if solar gain was more than needed.

Thermocouples used in this study were type T Cu-Const (Copper-Constantan) which had the capability of measuring temperature in the range of (-200)-300 ^{o}C.

A data acquisition system was used to monitor the temperature values measured by thermocouples. There were two 32-channel dataloggers and they could read the inputs of V(volt), A(amper), TCCJ(thermocouple with compensation), TC(thermocouple without compensation) and RT(resistance thermometer). Data were sent and saved from the dataloggers to a computer by a software program.

On the pipes of the heat pump, thermocouple ends were inserted in capillary copper tubes. These capillary tubes were embedded in the pipes that the refrigerant flowed by being closed one sides. So, the effects of surroundings on the temperature measurements of the refrigerant were minimized.

Glass thermometers were used to measure inlet and outlet temperatures of the tank, inlet and outlet temperatures of the room and the temperatures of the fan coil unit. These temperatures were also measured by thermocouples and thus accuracy of the values were checked.

Temperature gages were used to measure the inlet and outlet temperatures of the collector. These temperatures were needed to obtain the efficiency of the collector. Gages were the original equipments of the collector system and hence the usage of the thermocouple or glass thermometer was not needed.

The inlet and outlet temperatures of the air at the condenser were measured by the thermoanemometer. Velocity of the air was also measured by this device in m/s.

Figure 4.4 Some views of the temperature measurement devices.

4.2.2 Pressure Measurement

It is not sufficient to know the temperature of the refrigerant at some states, especially at subcooled and superheated states. Pressures are also needed for calculations. Pressure transducers were used at the inlet and the outlet of the evaporator and the condenser unit.

Cole-Parmer Model 68075 pressure transducers have 9-28 VDC (24 V recommended) excitation and 4-20 mA output and can measure in the range of 0-1000 psi (0-6895 kPa). The operating temperature limits are (-40)-127 ^{o}C.

The datalogger can take data from the pressure transducers because the transducers have 4-20 mA input. The connection of pressure transducers to the datalogger were made by a power supply unit that could give a 24 V DC input. Electrical installation guide of the device was utilized to make the connection.

T-fittings were used for the connection of pressure transducers to the copper pipes of the heat pump. They were made of brass material because of being stronger to keep its shape after a welding process.

4.2.3 Flow Rate Measurement

There were three flow rates to measure in the experimental setup: the refrigerant flow rate in the heat pump system, the water flow rate in the solar heating system and the air flow rate at the inlet or the outlet of the condenser. The mass flow rates were needed to have an idea about the energy transfers as a manner of power.

Krohne rotometer was used for measuring the mass flow rate of the refrigerant. It has a measurement range of 25-250 l/h (liter per hour). It was located at the outlet of the condenser since the refrigerant had the lowest quality at that location. Knowing pressure and temperature and thus the density of the refrigerant at that location, the mass flow rate of the refrigerant can be calculated in unit of kg/s.

The volumetric flow rate of water in the solar heating system were measured by the water flowmeter provided by Viessmann Company. The measurement range of it was 0-14 l/min (liter per minute). The mass flow rate of the water can be determined by multiplying volumetric flow rate value on the scale with the density of the liquid water at the corresponding temperature. The power input of the pump was 65 W.

The fan of the condenser took air inside the room from the top of the condenser and blew it from the bottom of the condenser at a certain velocity according to the level. It has a maximum power of 50 W. Thermoanemometer was used to measure the air velocity. Temperatures were also measured by this thermoanemometer at the inlet

and the outlet ducts of the condenser. The density of the air and the area of the duct at inlet or outlet were also needed to determine the mass flow rate of the air. The density can be determined from air tables at the corresponding temperature.

4.2.4 Power Input Measurement

A counter (wattmeter) was mounted on the wall inside the room to measure the consumption of electric power of the compressor and the fan in kW-h. The counter values were looked at the beginning and the end of each operation of the heat pump. The difference between the readings denoted the total consumption of electric power during that operation. Starting and end times for each operation were recorded in order to calculate the consumption in kW.

4.2.5 Solar Energy Gain

Pyranometer was used to measure the total radiation. A RMS digital milivoltmeter was used to read the total radiation as mV. Then the following equality was used to convert the unit to W/m^2 which was the unit of solar energy per unit area. Figure 4.5 shows the views of the pyranometer and the milivoltmeter.

$$11.17x10^{-3}\ mV=1\ W/m^2 \text{ or } 1\ mV=89.53\ W/m^2$$

Figure 4.5 Views of the pyranometer and the milivoltmeter.

4.3 Test Procedure

Preparations and arrangements should be done before the system is operated. The pyranometer is located in its place parallel to the solar collector that makes 45^{o} with the horizontal axis. One of the glass thermometers is placed outside the room. The main power switch is turned on. Then the switch of the power supply is opened. Thermocouple and pressure transducer placements are checked to make sure that there is no problem for working properly.

Inlet and outlet temperatures of the room are recorded as first data. The wattmeter is read and its value is recorded. The cable of the pyranometer is plugged to the multimeter and the first value of the total radiation on the tilted collector surface is recorded. USB-Serial Adapter is plugged into a computer to transfer the data from the datalogger to the computer. The recording frequency and period of the channels which is used to read temperature or pressure are regulated.

The temperatures of the tank and the collector at the inlet and the outlet are also recorded before operations. The inlet and the outlet valves of the tank and the collector are opened. The pump of the solar system is put in operation. The temperature regulations of the thermostats that control electrical heaters in the tank are checked. The power switch of the heat pump is turned on. Then the heat pump can be started.

The total solar radiation is recorded periodically and the pressures and the temperatures are checked occasionally during the operation. The inlet and the outlet temperatures of the air and velocities at the condenser are measured and recorded periodically.

All the measurements mentioned above are also taken at the end of the operation. The experimental results are listed and used in the analysis of the performance of the system. Electrical heater is regulated and all switches are turned off after experiments are finished for a day.

4.4 Experimental Results

A number of tests were performed inside the solar house at the Department of the Mechanical Engineering in METU, Ankara during the period of 8-23 November 2006. The effects of the tank temperature on the coefficient of performance of the heat pump, the collector efficiency and heat transfers at the evaporator and the condenser were investigated.

Figure 4.6 shows the variation of the evaporation temperature with respect to the tank temperature. It can be obviously seen in the figure that when the tank temperature increases the evaporation temperature of the heat pump cycle increases. That means that the evaporation in the heat pump cycle takes place at a higher temperature if the temperature of the heat source is higher. The temperature of the tank changes between 9-34.8 ^{o}C and the evaporation temperature has a range of 5.2-20.7 ^{o}C during the experiments. The change is almost linear. The temperature of the tank is not allowed to increase to higher values since the compressor can be damaged by exceeding its operation limits. The performance characteristics of the system have been investigated in this range.

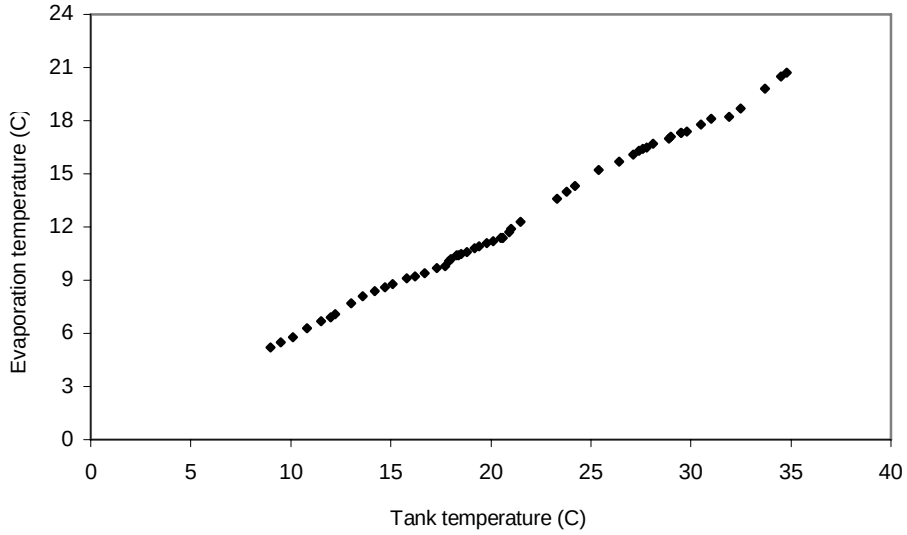

Figure 4.6 Variation of the evaporation temperature with the storage tank temperature.

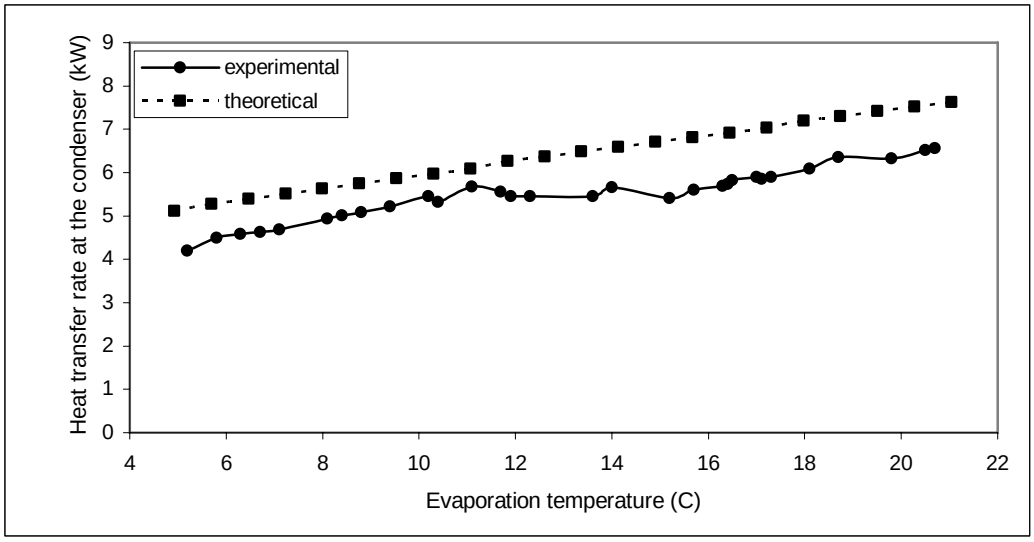

Figure 4.7 The effect of the evaporation temperature on the heat transfer rate at the condenser.

The effect of the evaporation temperature on the heat transfer rate at the condenser is presented in Figure 4.7. It can be seen from the figure that heat transfer rate at the condenser increases theoretically and experimentally when the evaporation temperature increases. This is mainly due to the increase in the mass flow rate of the refrigerant (Figure 4.8).

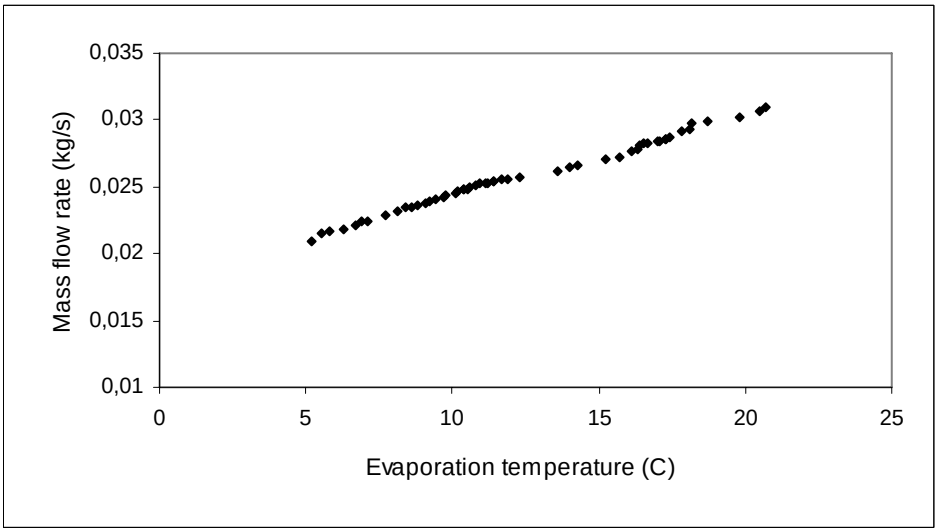

Figure 4.8 Variation of the refrigerant flow rate with the evaporation temperature.

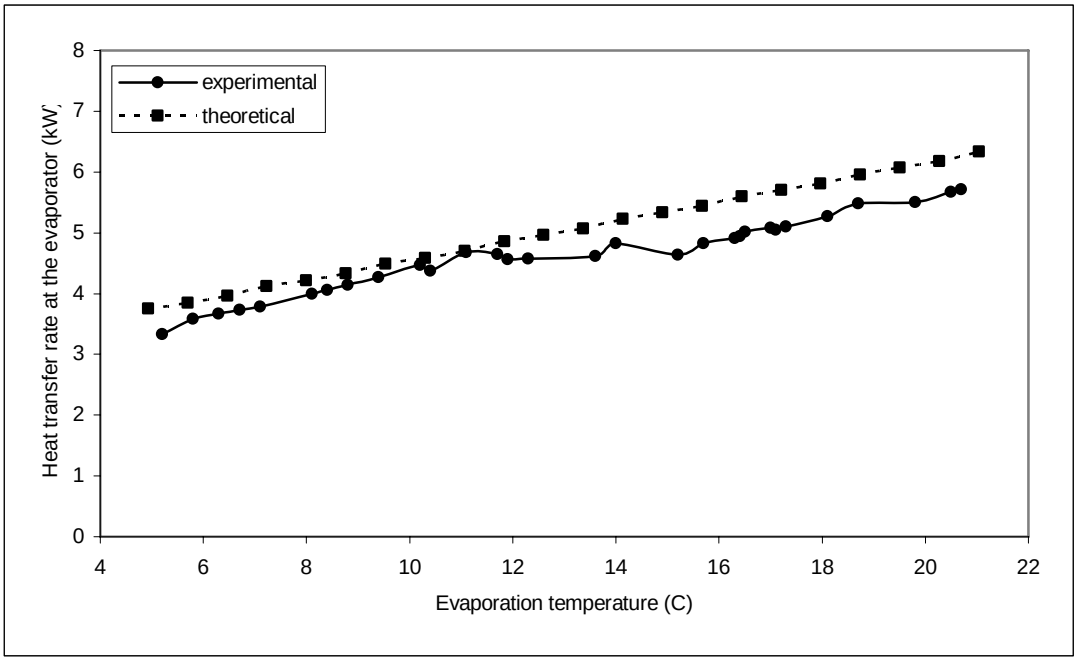

Figure 4.9 Variation of the heat transfer rate at the evaporator with the evaporation temperature.

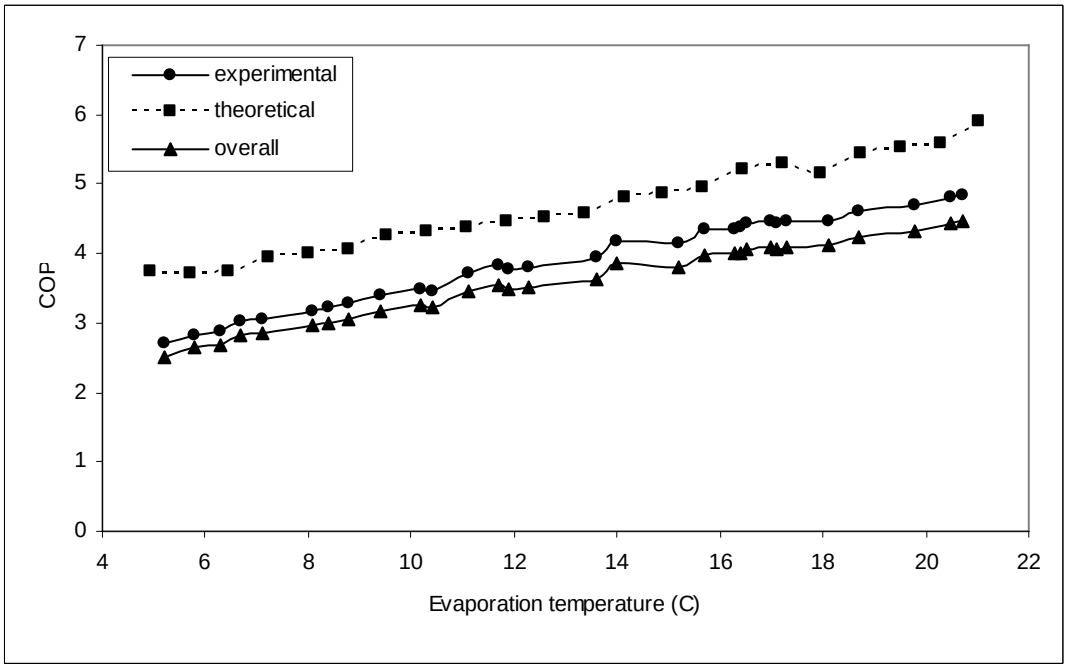

Figure 4.10 The effect of the evaporation temperature on COP values.

Heat transfer rate at the evaporator also increases with the increasing evaporation temperature (Figure 4.9). This is also due to increasing mass flow rates and increasing enthalpy differences between the inlet and the outlet of the evaporator.

Figure 4.10 shows the variation of the COP value of the heat pump for theoretical and experimental studies with the evaporation temperature. The increase in the overall COP of the system can also be seen in the figure. When the tank temperature increases, the evaporation temperature increases due to the hot water in the storage tank as mentioned before. The amount of condensation rate, i.e. Q_H, increases with a higher evaporation temperature. The difference between the inlet and outlet reservoir temperatures also decreases. Thus, the COP of the heat pump increases with increasing evaporation temperature. The maximum COP value reaches 4.85 for the experimental results and 6.14 for the theoretical predictions. 4.47 overall COP value was obtained when other work inputs, i.e. the consumptions of electric power of the fan of the condenser and the pump of the collector were taken into consideration.

The collector efficiency curve for both the experimental and the theoretical study can be seen in Figure 4.11. The efficiency of the collector decreases when the inlet temperature increases as mentioned before. The inlet temperature of the collector is almost same as the outlet temperature of the tank. Only 0.1-0.3 ^{o}C temperature differences occur between two locations. The efficiency of the collector is affected in inverse as contrary to the COP of the heat pump with increasing tank temperature. When the tank temperature decreases, the collector efficiency increases due to lower inlet temperature of the water to the collector. Furthermore, negligible convective heat losses of the evacuated tube collector bring about the high efficiency values. To minimize the bad effect of the high storage tank temperature on the collector efficiency an optimization can be made between the 18-25 ^{o}C tank temperatures at which COP values changes between 3.5-4.15 and collector efficiencies change in the range of 0.751-0.71.

Figure 4.12 shows the variation of measured data with time during the period of the experiments. Temperatures and radiation values are average values of that period on

an hour basis. The climatic conditions were not so good and the outlet temperature decreased about to 5 ^{o}C. Inlet temperatures were achieved to be kept above 15 ^{o}C most of the period.

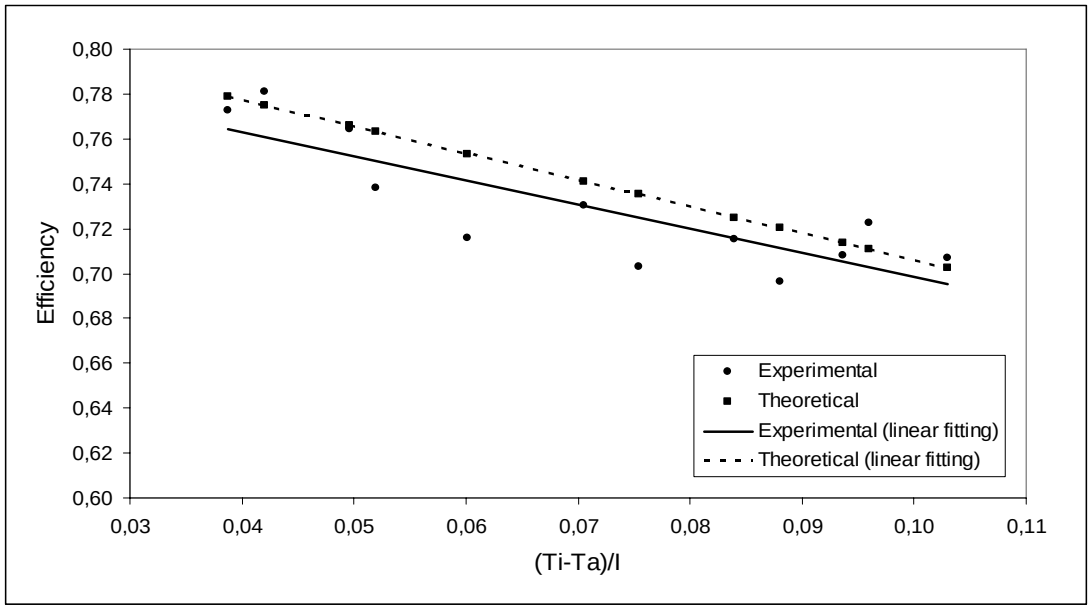

Figure 4.11 Experimental and theoretical collector efficiency curve.

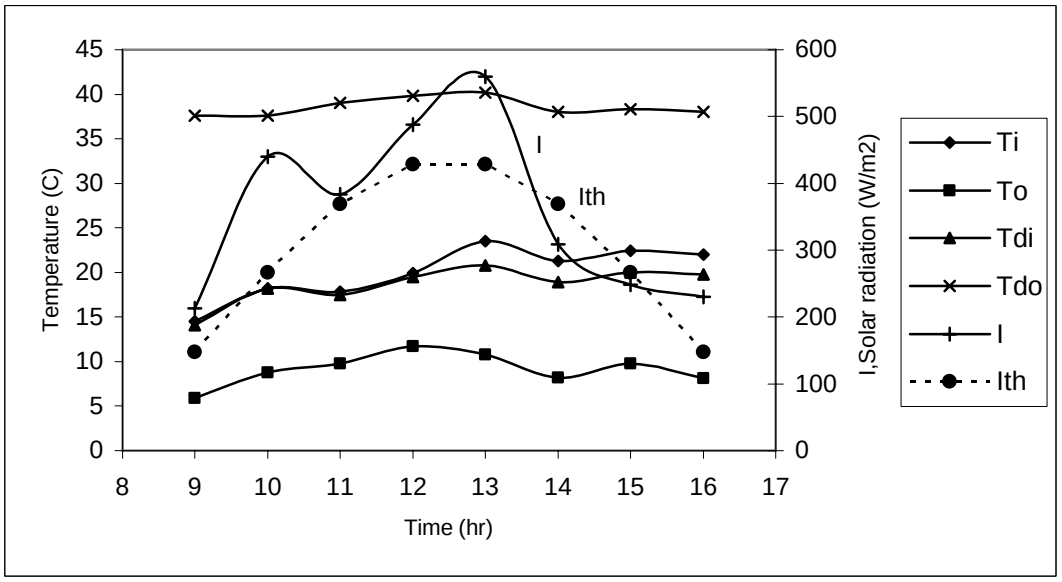

Figure 4.12 Variation of average solar radiation, room inlet and outlet temperatures and air duct inlet and outlet temperatures during the period of 8-23 November 2006.

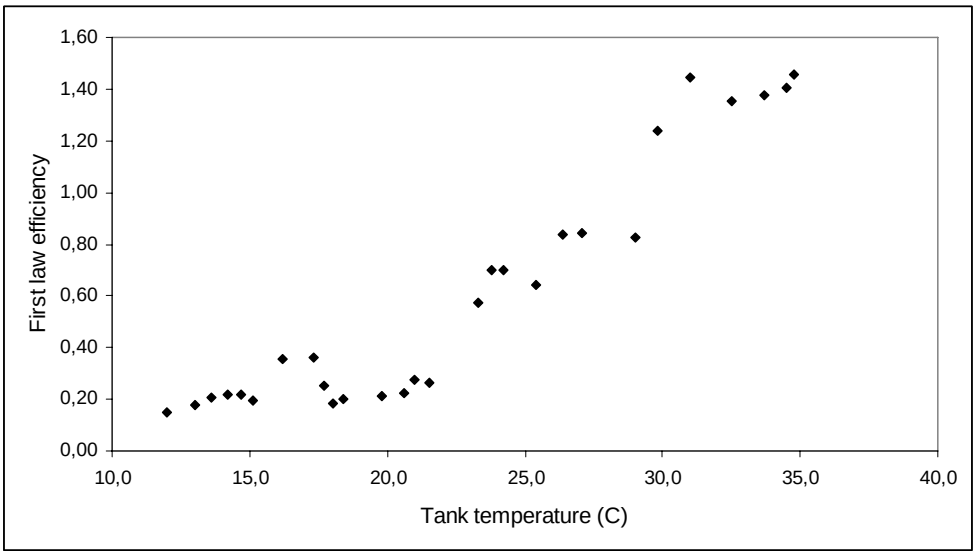

Figure 4.13 First law efficiency of the solar assisted heat pump system.

First law efficiency of the solar assisted heat pump is defined as the ratio of the heat rejected at the condenser in terms of the solar radiation to solar energy consumed by the compressor. It can be seen from Figure 4.13 that first law efficiency of the solar assisted heat pump system decreases by increasing the tank temperature. The tank temperature increases when solar gain increases, and this makes the collector less efficient. First law efficiency of the system can be formulated by:

$$\eta_I = \frac{I \cdot A_c \cdot Q_H}{Q_L \cdot W_c} \tag{4.1}$$

where I is the solar radiation in kW/m^2 and A_c is the collector area in m^2.

Figure 4.14 shows the variation of the second law efficiency of the system. When the temperature of the water in the tank increases, the second law efficiency first increases and has a maximum value of 0.28 and then decreases. The second law efficiency of the system can be defined as follows:

$$\eta_{II} = \frac{A_a + A_w}{A_s + W_c + W_p + W_f} \tag{4.2}$$

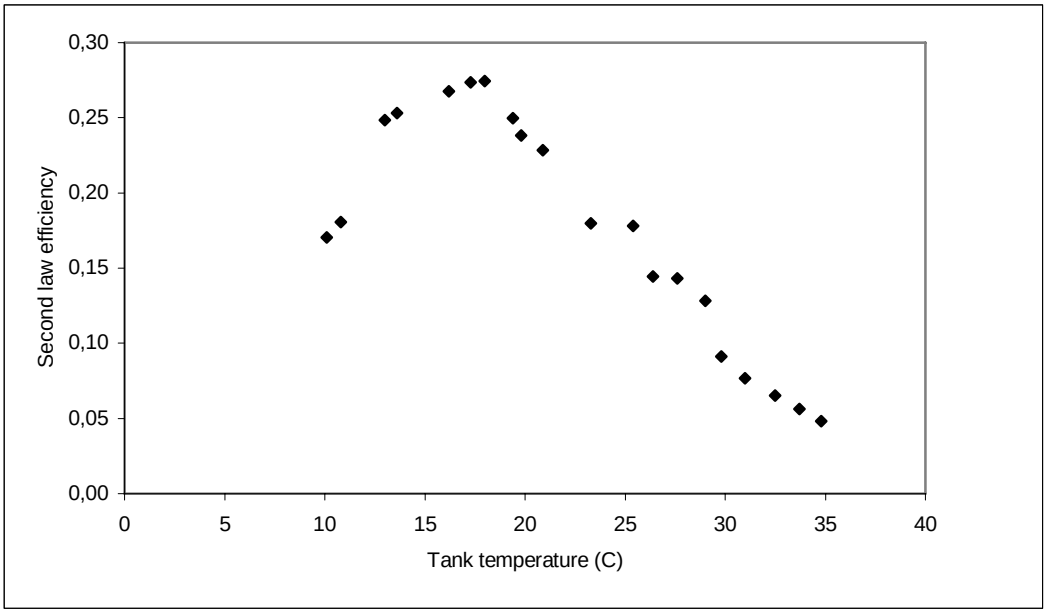

Figure 4.14 Second law efficiency of the solar assisted heat pump.

A_a is the exergy change of the air at the condenser and can be determined by:

$$A_a = m_a \cdot c_{pa} \cdot \left(T_2 - T_1 - T_0 \cdot \ln(\frac{T_2}{T_1}) \right) \tag{4.3}$$

where m_a is the mass flow rate of the air in kg/s and T_0 is ambient temperature in K. A_w is the exergy change of the water in the storage tank and can be calculated by:

$$A_w = m_w \cdot \left(u_2 - u_1 - T_0 \cdot (s_2 - s_1) \right) \tag{4.4}$$

where m_w is the mass flow rate of the water in kg/s. A_s is the exergy of solar radiation and can be determined by:

$$A_s = \frac{I \cdot A_c}{1000} \cdot \left(1 - \frac{T_0}{T_{effsun}} \right) \tag{4.5}$$

where T_{effsun} is effective sun temperature and can be taken 5780 K from the literature.

CHAPTER 5

CONCLUSIONS

In this study, a commercial air conditioner and an evacuated tube solar collector were used to setup a solar assisted heat pump. The evaporator of the air conditioner was disbanded and instead, a helical coil evaporator was constructed by copper tubes. Thus, solar assistance was achieved by inserting the new evaporator coil into a water storage tank. Energy was obtained from the solar collector to heat the water storage tank. Copper tube extensions and measurement devices were also added to the setup.

Experiments were made between 9-34.8 ^{o}C tank temperatures and a performance analysis of the system was carried out according to the experimental results. The COPs of the heat pump and the overall system, the heat transfer rates of the evaporator and the condenser, the efficiency of the collector and the exergetic efficiency of the solar assisted heat pump system were calculated. Saturated and superheated properties for R407C were determined from the tables of thermodynamic properties in the analysis of the characteristics of the system.

The temperature of the tank was not increased more than 35 ^{o}C to avoid damaging the compressor of the heat pump. The increase in the tank temperature also caused to decrease in the efficiency of the collector and it was not a desired case. An optimum temperature range of the tank should be selected for a certain period and space so that the performance of the heat pump and the collector efficiency are satisfactory.

The experimental setup was designed for the winter conditions to obtain enough heat which would be transferred to the heated space and it might not give desired effects at warmer conditions of the weather. Higher compressor works or lower COP values could be obtained for a cooling operation.

The tilted angle of the collector was 45^o during the experiments. This angle was selected for a longer-term study and the optimum angle for this short-term study in winter could be increased by 10-15^o to gain more solar radiation. Besides, a tracking system for the collector could also be used to increase the solar energy gain.

It was an assumption to keep the temperature of the tank constant during the evaporation process of the vapor compression heat pump cycle. Larger tank volume capacities, i.e. larger spaces, are needed to verify this assumption (120 kg.). If many residences are considered to heat, wider sources such as a pond are needed to keep the temperature of the source at constant temperature.

Copper tube extensions were needed to connect the components (the evaporator, the condenser and the compressor) of the heat pump and 90^o turnings had to be done at some locations on the pipes. This caused to high pressure drops at the inlet of the compressor and affected the performance characteristics of the heat pump. The turnings should be made as less as possible to minimize the pressure drops. The insulation of the tubes was also important to prevent heat losses to the ambient.

The pressure transducers were calibrated by pressurized air by using 6-bar pressure gage. This pressure is very small for a vapor compression cycle. The higher pressures are needed for an appropriate calibration of the pressure transducers. It was not possible to supply higher pressures for well calibration in the existing opportunities.

For future works, a dual-source solar assisted heat pump can be designed and constructed and thus an appropriate heat source can be selected to obtain more efficient system. Besides, the applicability of a series system that was the system used in this study can be tested at different location in Turkey for a widespread usage of series systems. Furthermore, an economic analysis is also needed for proving of the profitability of the series system for a long-term period by taking the investment and operating costs of the system into consideration. A rise in the cost of electricity brings about the increase in the profitability of a solar assisted heat pump because of the reduction in the consumption of electricity for a long-term operating period.

REFERENCES

[1] H. A. Ingley, S. K. Wang, A. Rabl, Air Conditioning and Refrigeration, The CRC Handbook of Mechanical Engineering, 2th ed., *CRC Press*, (2005)

[2] Technical Series Heat Pumps, *Viessmann*, 2004, *www.viessmann.co.uk/downloads/TechnicalSeriesHeatPumps.pdf*, Last Access Date:15.12.2006.

[3] Y. A. Çengel, M. A. Boles, Thermodynamics: An Engineering Approach, *McGraw-Hill International Editions*, 1989.

[4] H. L. von Cube, F. Steimle, Heat Pump Technology, *Butterworths*, London, 1981.

[5] H. J. Sauer and R. H. Howell, Heat Pump Systems, *John Wiley & Sons*, New York, 1983.

[6] B. Acıkalın, Construction and Performance Analysis of an Air-to-Air and Solar Assisted Heat Pump, Mechanical Engineering, *METU*, (1993).

[7] P. Sporn, E. R. Ambrose, T. Baumeister, Heat Pumps, *John Wiley & Sons Inc.*, 1947.

[8] HVAC handbook, (1987).

[9] O. Ozgener and A. Hepbasli, A review on the energy and exergy analysis of solar assisted heat pump ssytems, *Renewable and Sustainable Energy Reviews*, xx (2005) 1-16.

[10] R. Yamankaradeniz and I. Horuz, The theoretical and experimental investigation of the characteristics of solar-assisted heat pump for clear days, *Int. Comm. Heat Mass Transfer*, 25/6 (1998) 885-898.

[11] B. J. Huang and J. P. Chyng, Integral-type solar assisted heat pump, *Renewable Energy*, 16 (1999) 731-734.

[12] J. G. Cervantes and E. Torres-Reyes, Experiments on a solar-assisted heat pump and an exergy analysis of the system, *Applied Thermal Engineering*, 22 (2002) 1289-1297.

[13] O. Ozgener and A. Hepbasli, Performance analysis of a solar-assisted ground-source heat pump system for greenhouse heating: an experimental study, *Building And Environment*, 2004.

[14] H. Hulin, G. Xinshi and S. Yuehong, Theoretical thermal performance analysis of two solar-assisted heat-pump systems, *International Journal of Energy Research*, 23 (1999) 1-6.

[15] H. Z. Abou-Ziyan, et al., Solar-assisted R22 and R134a heat pump system for low-temperature applications, *Applied Thermal Engineering*, 17/5 (1997) 455-469.

[16] Y. H. Kuang, R. Z. Wang, L. Q. Yu, Experimental study on solar assisted heat pump system for heat supply, *Energy Conversion and Management*, 44 (2003) 1089-1098.

[17] S. K. Chaturvedi, D. T. Chen, A. Kheireddine, Thermal performance of a variable capasity direct expansion solar-assisted heat pump, *Energy Conversion and Management*, 39/3/4 (1998) 181-191.

[18] M. N. A. Hawlader, S. K. Chou, M. Z. Ullah, The performance of a solar assisted heat pump water heating system, *Applied Thermal Engineering*, 21 (2001) 1049-1065.

[19] V. Badescu, Model of a thermal storage device integrated into a solar assisted heat pump system for space heating, *Energy Conversion and Management*, 44 (2003) 1589-1604.

[20] B. J. Huang, C. P. Lee, Long-term performance of solar-assisted heat pump water heater, *Renewable Energy*, 29 (2003) 633-639.

[21] S. Göktun and İ. D. Er, The optimum performance of a solar-assisted combined absorption-vapor compression system for air conditioning and space heating, *Solar Energy*, 71/3 (2001) 213-216.

[22] R. Yumrutaş, Ö. Kaşka, Experimental investigation of thermal performance of a solar assisted heat pump system with an energy storage, *International Journal Of Energy Research*, 28 (2004) 163-175.

[23] J. A. Duffie, W. A. Beckman, Solar Engineering Of Thermal Processes, *John Wiley&Sons*, Inc., 1991.

[24] J. S. Hsieh, Solar Energy Engineering, *Prentice-Hall Press*, 1986.

[25] Viessmann Company, *www.viessmann.co.uk/downloads/Vitosol-300-Datasheet.pdf*, Last Access Date: 15.12.2006.

[26] K. C. Ng, C. Yap, T. H. Khor, Outdoor testing of evacuated-tube heat pipe solar collectors, *Proc Instn Mech Engrs*, 214 (2000) 23-30.

[27] F. P. Incropera, D. P. Dewitt, Fundamentals of Heat and Mass Transfer, 3rd ed., *Wiley*, 1990.

[28] J. P. Holman, Heat Transfer, 4th ed., *McGraw-Hill*, 1976.

[29] J. R. Thome, Engineering Data Book III, *Wolverine Tube, Inc.*, 2006.

[30] H. Yüncü, S. Kakaç, Temel Isı Trasferi, *Bilim Yayıncılık*, Ankara, 1999.

APPENDIX A

FIGURES AND TABLES FOR THE EXPERIMENTS

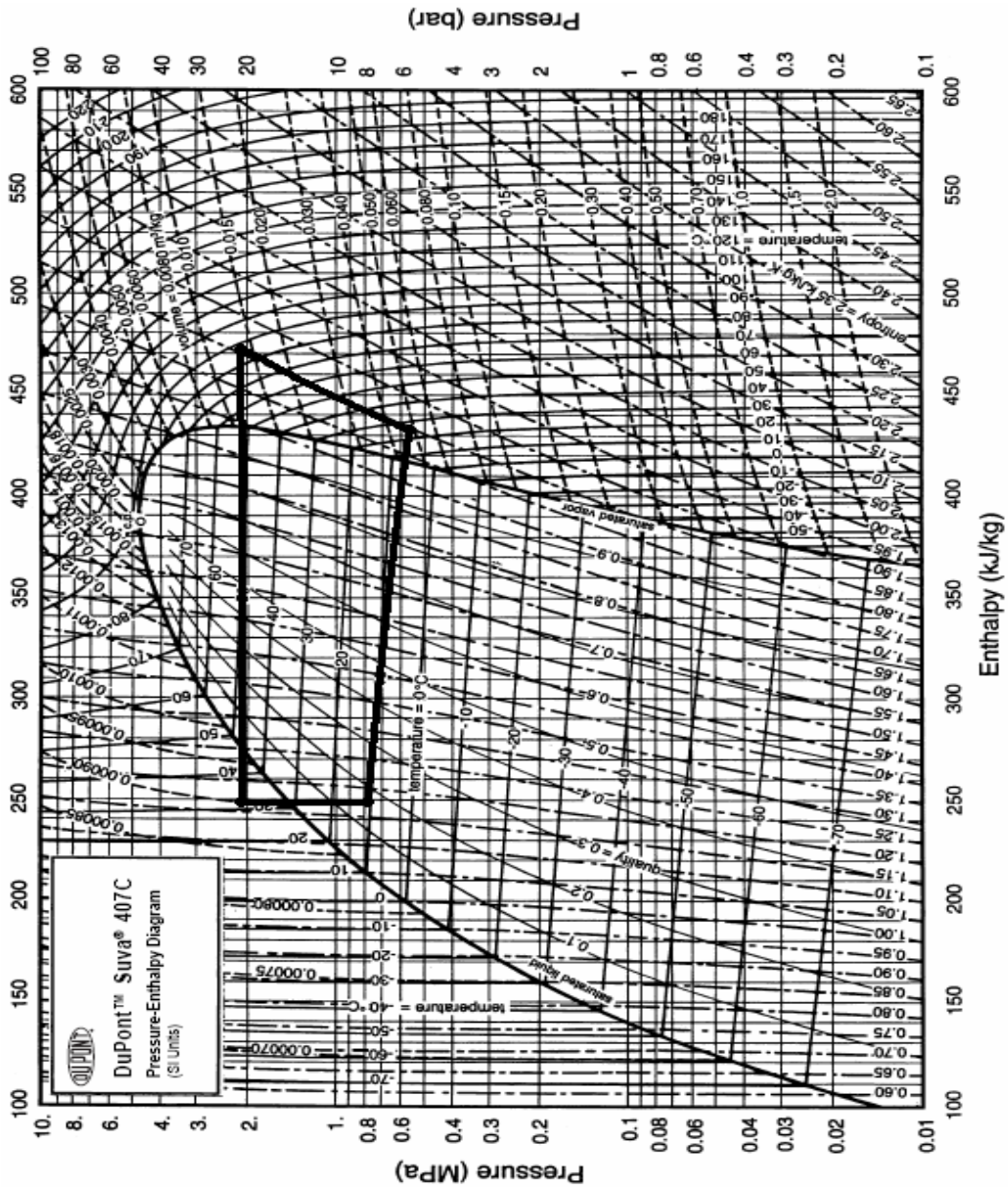

Figure A.1 Pressure-Enthalpy diagram of R407C for the experiment on 11.11.2006 at 16:31-16:40

Table A.1 Results for the experiment on 08.11.2006

Time	Counter (kWh)	P_1 (kPa)	P_2 (kPa)	P_3 (kPa)	P_4 (kPa)	T_1 (^oC)	T_2 (^oC)	T_3 (^oC)	T_4 (^oC)	m kg/s	T_{in} (^oC)	T_{out} (^oC)	T_{di} (^oC)	T_{do} (^oC)	T_t (^oC)	T_{ci} (^oC)	T_{co} (^oC)
Start 10:44:30	163,37										16,2	8,7					
End 10:52:32	163,56	740	2597	2581	954	43,6	96,7	43,1	18,2	0,0298	19	8,8	20,1	40	31,9	31,7	32,5
Start 11:12:40	163,58										15,7	10,5					
End 11:19:50	163,75	704	2556	2540	942	42,4	95,8	41,9	17,8	0,0291	19,1	9,6	20,3	39,8	30,5	30,3	31,1
Start 11:36:00	163,77										16,7	9,8					
End 11:44:45	163,97	622	2641	2629	909	42,5	97,4	43,5	17,3	0,0286	21	9,9	20,2	40,2	29,5	29,4	30,2
Start 12:03:42	163,99										16,6	9,9					
End 12:12:27	164,19	598	2495	2480	897	40,8	94,6	43,0	17,1	0,0284	21	9,8	20,5	40,4	29	28,8	29,8
Start 12:31:24	164,21										16,6	9,5					
End 12:39:46	164,40	590	2425	2390	874	38,1	91,7	42,8	16,4	0,0281	21,5	10,3	20,3	39,9	27,6	27,5	28,2
Start 13:04:34	164,42										16,8	10,2					
End 13:13:23	164,62	686	2349	2178	885	37,7	89,3	40,7	16,5	0,0282	21,8	9,9	19,8	40,1	27,8	27,7	28,3
Start 13:42:40	164,64										18,1	9,3					
End 13:52:25	164,86	559	2443	2397	864	38,3	92,3	42,7	16,3	0,0278	22,4	9,3	20,2	40,6	27,4	27,2	27,9
Start 14:20:52	164,88										16,2	9,6					
End 14:30:37	165,10	552	2384	2370	830	37,3	91,3	45,0	15,2	0,0270	21,3	9,6	20,5	40,7	25,4	25,3	26,0
	W (kW)	h_1 (kj/kg)	h_2 (kj/kg)	$h_3=h_4$ (kj/kg)	Q_L (kW)	Q_H (kW)	T_t (^oC)	I (W/m^2)	COP	η_{col}	η_{colth}	COP_{ove}	Q_{Lth} (kW)	Q_{Hth} (kW)	COP_{th}	Q_{us} (kW)	
10:44:30-10:52:32	1,37	447,4	475,7	269,0	5,32	6,16	31,9	381	4,50	0,716	0,753	4,15	10,37	12,52	5,82	0,54	
11:12:40-11:19:50	1,37	446,8	475,3	266,9	5,24	6,07	30,5	398	4,42	0,729	0,763	4,08	9,62	11,68	5,65	0,58	
11:36:00-11:44:45	1,32	448,0	475,9	269,8	5,10	5,89	29,5	403	4,46	0,721	0,767	4,10	9,24	11,36	5,35	0,58	
12:03:42-12:12:27	1,32	446,8	474,8	268,9	5,05	5,85	29	470	4,42	0,734	0,777	4,07	9,01	11,11	5,30	0,69	
12:31:24-12:39:46	1,31	444,5	472,6	268,5	4,95	5,73	27,6	358	4,37	0,710	0,768	4,02	8,48	10,59	5,02	0,51	
13:04:34-13:13:23	1,31	442,8	471,0	264,8	5,02	5,82	27,8	313	4,43	0,696	0,757	4,08	8,56	10,66	5,07	0,44	
13:42:40-13:52:25	1,30	445,1	473,0	268,4	4,91	5,69	27,4	345	4,36	0,738	0,763	4,01	8,40	10,54	4,93	0,51	
14:20:52-14:30:37	1,30	444,3	472,7	272,5	4,64	5,41	25,4	358	4,15	0,710	0,773	3,81	7,72	9,78	4,75	0,51	

Table A.2 Results for the experiment on 09.11.2006

Time	Counter (kWh)	P_1 (kPa)	P_2 (kPa)	P_3 (kPa)	P_4 (kPa)	T_1 (^oC)	T_2 (^oC)	T_3 (^oC)	T_4 (^oC)	m kg/s	T_{in} (^oC)	T_{out} (^oC)	T_{di} (^oC)	T_{do} (^oC)	T_t (^oC)	T_{ci} (^oC)	T_{co} (^oC)
Start 10:25:18	165,11										13,7	10,6					
End 10:35:39	165,35	720	2468	2453	931	41,1	93,4	41,2	17,4	0,0287	19,8	11,4	19,6	40,1	29,8	29,7	31,1
Start 10:55:08	165,37										14,3	11,4					
End 11:05:45	165,62	721	2583	2569	941	43,1	96,2	42,2	18,1	0,0293	20,1	12,4	20	40,5	31	30,8	32,5
Start 11:27:57	165,64										14,6	12,5					
End 11:38:51	165,90	784	2548	2530	967	42,4	95,1	39,3	18,7	0,0299	19,4	13,2	19,1	40,3	32,5	32,4	34,0
Start 12:01:30	165,92										15,3	13,2					
End 12:12:37	166,18	733	2715	2698	991	48,1	101,3	41,6	20,5	0,0306	20,4	13,4	20,2	41	34,5	34,3	35,9
Start 12:33:13	166,20										16	13,4					
End 12:43:28	166,44	789	2704	2685	1001	48,8	100,9	41,7	20,7	0,0309	20,5	14,2	20,3	40,5	34,8	34,7	36,4
Start 13:06:38	166,46										21,4	11,8					
End 13:17:22	166,71	785	2650	2632	980	45,7	97,8	41,8	19,8	0,0302	25,1	11,7	21,7	40,2	33,7	33,6	35,2
Start 15:38:50	166,73										20,8	11,6					
End 15:50:22	166,99	516	2536	2520	853	39,9	95,4	44,7	16,1	0,0276	26,8	10,9	21,5	40,1	27,1	27	28,0
Start 16:14:45	167,01										19,7	9,3					
End 16:26:49	167,28	569	2485	2470	842	39,8	94,5	43,0	15,7	0,0272	26,5	8,7	20,9	40	26,4	26,2	27,1
	W (kW)	h_1 (kj/kg)	h_2 (kj/kg)	$h_3=h_4$ (kj/kg)	Q_L (kW)	Q_H (kW)	T_t (^oC)	I (W/m^2)	COP	η_{col}	η_{colth}	COP_{ove}	Q_{Lth} (kW)	Q_{Hth} (kW)	COP_{th}	Q_{us} (kW)	
10:25:18-10:35:39	1,34	445,4	473,9	265,7	5,16	5,97	29,8	716	4,45	0,730	0,795	4,10	9,39	11,46	5,52	1,05	
10:55:08-11:05:45	1,36	447,2	475,4	267,4	5,27	6,09	31	851	4,47	0,726	0,799	4,12	9,77	11,84	5,72	1,23	
11:27:57-11:38:51	1,38	445,7	474,6	262,3	5,48	6,35	32,5	806	4,60	0,721	0,797	4,24	10,45	12,57	5,92	1,16	
12:01:30-12:12:37	1,35	451,6	479,3	266,3	5,67	6,52	34,5	828	4,81	0,710	0,795	4,44	10,60	12,68	6,09	1,18	
12:33:13-12:43:28	1,35	451,5	479,0	266,6	5,71	6,56	34,8	859	4,85	0,706	0,797	4,47	10,67	12,75	6,14	1,21	
13:06:38-13:17:22	1,35	448,7	476,2	266,7	5,50	6,33	33,7	806	4,69	0,721	0,793	4,33	10,52	12,62	6,02	1,16	
15:38:50-15:50:22	1,30	447,1	475,1	272,0	4,83	5,61	27,1	475	4,30	0,727	0,785	3,95	8,33	10,47	4,89	0,69	
16:14:45-16:26:49	1,29	446,3	474,9	268,9	4,82	5,60	26,4	466	4,34	0,734	0,780	3,98	8,10	10,23	4,81	0,68	

Table A.3 Results for the experiment on 11.11.2006

Time	Counter (kWh)	P_1 (kPa)	P_2 (kPa)	P_3 (kPa)	P_4 (kPa)	T_1 (^oC)	T_2 (^oC)	T_3 (^oC)	T_4 (^oC)	m kg/s	T_{in} (^oC)	T_{out} (^oC)	T_{di} (^oC)	T_{do} (^oC)	T_t (^oC)	T_{ci} (^oC)	T_{co} (^oC)
Start 14:10:42	167,30										11,8	9					
End 14:29:12	167,51	480	2154	2139	784	30,7	89,5	38,9	12,3	0,0257	21,1	7,6	19,5	34,9	21,5	21,4	21,7
Start 14:51:35	167,53										13,5	8,5					
End 15:00:24	167,75	467	2116	2101	785	29,8	88,9	38,0	11,9	0,0255	21,2	8,3	19,8	33,9	21	20,8	21,1
Start 15:24:23	167,77										12,4	8,1					
End 15:33:51	168,01	535	2104	2090	783	28,5	88,7	33,3	11,4	0,0254	21	7,5	20	35	20,6	20,5	20,8
Start 15:59:47	168,03										12,2	7,6					
End 16:07:49	168,24	563	2097	2085	780	26,9	88,3	32,1	11,2	0,0253	20,9	7,5	20,2	35,5	20,1	20	20,3
Start 16:31:40	168,26										12,5	7,2					
End 16:40:29	168,49	566	2065	2050	775	25,8	87,4	32,3	10,8	0,0251	20,5	6,9	20,4	35,3	19,2	19	19,3
Start 16:48:30	168,51										12,6	6,6					
End 16:56:50	168,73	517	2039	2025	775	23,7	86,9	31,2	10,4	0,0248	20	6,5	20,5	34,8	18,4	18,3	18,6
	W (kW)	h_1 (kj/kg)	h_2 (kj/kg)	$h_3=h_4$ (kj/kg)	Q_L (kW)	Q_H (kW)	T_t (^oC)	I (W/m^2)	COP	η_{col}	η_{colth}	COP_{ove}	Q_{Lth} (kW)	Q_{Hth} (kW)	COP_{th}	Q_{us} (kW)	
14:10:42-14:29:12	1,43	439,5	474,0	261,6	4,57	5,46	21,5	157	3,81	0,697	0,720	3,53	6,97	8,95	4,51	0,22	
14:51:35-15:00:24	1,45	438,9	473,8	260,0	4,56	5,45	21	166	3,77	0,703	0,735	3,49	6,89	8,90	4,43	0,23	
15:24:23-15:33:51	1,47	436,8	473,8	251,8	4,70	5,64	20,6	139	3,83	0,708	0,714	3,56	6,97	9,09	4,28	0,20	
15:59:47-16:07:49	1,52	435,0	473,5	249,8	4,68	5,66	20,1	134	3,73	0,731	0,714	3,47	6,74	8,87	4,16	0,20	
16:31:40-16:40:29	1,52	434,0	472,9	250,2	4,61	5,59	19,2	130	3,69	0,757	0,714	3,43	6,36	8,47	4,01	0,20	
16:48:30-16:56:50	1,53	433,0	472,7	248,3	4,58	5,57	18,4	125	3,63	0,755	0,713	3,37	6,06	8,19	3,84	0,19	

Table A.4 Results for the experiment on 12.11.2006

Time	Counter (kWh)	P_1 (kPa)	P_2 (kPa)	P_3 (kPa)	P_4 (kPa)	T_1 (^oC)	T_2 (^oC)	T_3 (^oC)	T_4 (^oC)	m kg/s	T_{in} (^oC)	T_{out} (^oC)	T_{di} (^oC)	T_{do} (^oC)	T_t (^oC)	T_{ci} (^oC)	T_{co} (^oC)
Start 14:41:18	168,75										8,9	6,6					
End 14:50:25	168,99	590	2072	2060	783	26,2	87,7	31,6	11,1	0,0253	17,1	6,5	14,5	37,5	19,8	19,6	19,9
Start 15:09:12	169,01										9,2	6,4					
End 15:19:25	169,28	590	2050	2034	775	25,4	87,1	31,2	10,6	0,0249	17	6,3	15,4	37,4	18,8	18,6	18,9
Start 15:35:33	169,30										9,9	6,3					
End 15:45:15	169,56	523	2007	1992	754	23,7	86,6	33,1	10,2	0,0246	16,8	6,3	15,1	38,6	18	18,7	18,9
	W (kW)	h_1 (kj/kg)	h_2 (kj/kg)	$h_3=h_4$ (kj/kg)	Q_L (kW)	Q_H (kW)	T_t (^oC)	I (W/m^2)	COP	η_{col}	η_{colth}	COP_{ove}	Q_{Lth} (kW)	Q_{Hth} (kW)	COP_{th}	Q_{us} (kW)	
14:41:18-14:50:25	1,53	434,0	473,1	249,0	4,68	5,67	19,8	134	3,71	0,732	0,709	3,45	6,59	8,71	4,10	0,20	
15:09:12-15:19:25	1,54	433,3	472,8	248,2	4,61	5,59	18,8	125	3,64	0,726	0,708	3,39	6,21	8,29	3,98	0,18	
15:35:33-15:45:15	1,56	432,8	472,8	251,4	4,46	5,45	18	116	3,50	0,751	0,698	3,26	5,91	8,07	3,73	0,17	

Table A.5 Results for the experiment on 13.11.2006

Time	Counter (kWh)	P_1 (kPa)	P_2 (kPa)	P_3 (kPa)	P_4 (kPa)	T_1 (^oC)	T_2 (^oC)	T_3 (^oC)	T_4 (^oC)	m kg/s	T_{in} (^oC)	T_{out} (^oC)	T_{di} (^oC)	T_{do} (^oC)	T_t (^oC)	T_{ci} (^oC)	T_{co} (^oC)
Start 14:21:36	169,58										13,4	9,2					
End 14:30:01	169,79	453	2140	2125	786	29	89,3	35,9	11,7	0,0255	19,8	9,1	19,6	39,7	20,9	20,7	20,9
Start 14:50:25	169,81										12,5	9					
End 14:58:46	170,02	494	2085	2071	783	27,6	88,2	32,2	11,4	0,0254	20,2	8,8	19,8	40,2	20,5	20,3	20,5
Start 15:18:33	170,04										13,1	8,8					
End 15:28:39	170,3	592	2063	2049	782	25,9	86,9	31,2	10,9	0,0252	20,6	8,7	19,9	40,1	19,4	19,3	19,5
Start 15:47:57	170,32										12,2	8,9					
End 15:56:36	170,55	560	2053	2038	776	24,9	87,3	32,1	10,5	0,0248	19,5	9	19,3	40	18,5	18,4	18,6
Start 16:15:42	170,57										11,5	9,1					
End 16:24:20	170,80	511	1984	1970	743	23,6	85,3	36,7	10,1	0,0245	18,5	8,7	18,7	39,6	17,9	17,8	18,0
	W (kW)	h_1 (kj/kg)	h_2 (kj/kg)	$h_3=h_4$ (kj/kg)	Q_L (kW)	Q_H (kW)	T_t (^oC)	I (W/m^2)	COP	η_{col}	η_{colth}	COP_{ove}	Q_{Lth} (kW)	Q_{Hth} (kW)	COP_{th}	Q_{us} (kW)	
14:21:36-14:30:01	1,45	438,4	474,0	256,2	4,65	5,55	20,9	121	3,83	0,722	0,711	3,55	6,97	9,04	4,359	0,1746	
14:50:25-14:58:46	1,46	436,6	473,5	250,0	4,74	5,68	20,5	112	3,89	0,715	0,703	3,61	6,89	9,02	4,232	0,1601	
15:18:33-15:28:39	1,49	433,7	472,4	248,3	4,67	5,65	19,4	103	3,78	0,707	0,702	3,51	6,44	8,54	4,057	0,1456	
15:47:57-15:56:36	1,55	433,3	473,0	249,7	4,55	5,54	18,5	112	3,58	0,716	0,725	3,34	6,06	8,11	3,945	0,1602	
16:15:42-16:24:20	1,55	432,9	471,8	257,7	4,29	5,24	17,9	94	3,39	0,736	0,710	3,15	5,91	8,13	3,659	0,1383	

Table A.6 Results for the experimental on 14.11.2006

Time	Counter (kWh)	P_1 (kPa)	P_2 (kPa)	P_3 (kPa)	P_4 (kPa)	T_1 (^oC)	T_2 (^oC)	T_3 (^oC)	T_4 (^oC)	m kg/s	T_{in} (^oC)	T_{out} (^oC)	T_{di} (^oC)	T_{do} (^oC)	T_t (^oC)	T_{ci} (^oC)	T_{co} (^oC)
Start 15:12:05	170,85										13,9	7					
End 15:20:20	171,04	688	2439	2424	921	40,5	92,7	41,1	17,3	0,0286	18,6	6,1	18,4	39,8	29,5	29,3	30,2
Start 15:36:18	171,06										15,5	6,5					
End 15:47:14	171,31	695	2465	2450	895	40,5	93,1	41,5	17	0,0284	20,1	6,6	18,7	40	28,9	28,7	29,3
Start 16:09:30	171,33										16,3	6,3					
End 16:19:38	171,56	600	2402	2387	889	38,6	91,5	42,6	16,7	0,0283	21	6	19,4	40,2	28,1	28	28,5
	W (kW)	h_1 (kj/kg)	h_2 (kj/kg)	$h_3=h_4$ (kj/kg)	Q_L (kW)	Q_H (kW)	T_t (^oC)	I (W/m^2)	COP	η_{col}	η_{colth}	COP_{ove}	Q_{Lth} (kW)	Q_{Hth} (kW)	COP_{th}	Q_{us} (kW)	
15:12:05-15:20:20	1,33	445,3	473,5	265,5	5,14	5,95	29,5	425	4,47	0,726	0,760	4,11	9,24	11,33	5,42	0,62	
15:36:18-15:47:14	1,32	445,2	473,6	266,2	5,08	5,89	28,9	313	4,45	0,730	0,741	4,10	9,01	11,16	5,20	0,46	
16:09:30-16:19:38	1,31	444,8	472,7	268,2	5,00	5,79	28,1	246	4,41	0,723	0,719	4,06	8,63	10,71	5,15	0,36	

Table A.7 Results for the experiment on 15.11.2006

Time	Counter (kWh)	P_1 (kPa)	P_2 (kPa)	P_3 (kPa)	P_4 (kPa)	T_1 (^oC)	T_2 (^oC)	T_3 (^oC)	T_4 (^oC)	m kg/s	T_{in} (^oC)	T_{out} (^oC)	T_{di} (^oC)	T_{do} (^oC)	T_t (^oC)	T_{ci} (^oC)	T_{co} (^oC)
Start 09:35:15	171,57										7,2	4,6					
End 09:43:35	171,79	548	1965	1950	765	24,7	84,7	36,3	10,4	0,0248	15,2	5,7	14,7	38,4	18,3	18,2	18,4
Start 09:57:25	171,81										8,1	5,8					
End 10:05:27	172,02	496	2025	2009	739	24,5	86,1	36,5	9,8	0,0244	16	5,7	15,6	38,7	17,7	17,6	17,9
Start 10:31:23	172,04										9,4	5,9					
End 10:40:15	172,27	486	2026	2007	737	24,1	86	36,1	9,7	0,0242	15,7	6,1	15	39,1	17,3	17,2	17,7
Start 10:57:56	172,29										10,5	6,4					
End 11:05:32	172,49	463	2103	2088	733	24,3	88,4	35,9	9,4	0,0240	15,5	6,2	15,3	38,9	16,7	16,6	17,2
Start 11:19:37	172,51										11,4	6,8					
End 11:28:40	172,75	485	2065	2051	721	24,2	87,7	37,5	9,2	0,0239	16,7	6,7	16,4	39,5	16,2	16,1	16,6
	W (kW)	h_1 (kj/kg)	h_2 (kj/kg)	$h_3=h_4$ (kj/kg)	Q_L (kW)	Q_H (kW)	T_t (^oC)	I (W/m^2)	COP	η_{col}	η_{colth}	COP_{ove}	Q_{Lth} (kW)	Q_{Hth} (kW)	COP_{th}	Q_{us} (kW)	
09:35:15-09:43:35	1,53	433,3	471,4	257,0	4,37	5,32	18,3	90	3,46	0,772	0,659	3,22	5,98	8,14	3,77	0,14	
09:57:25-10:05:27	1,52	433,9	472,1	257,3	4,31	5,24	17,7	157	3,45	0,743	0,735	3,21	5,98	8,27	3,62	0,23	
10:31:23-10:40:15	1,51	433,7	471,9	256,7	4,28	5,21	17,3	224	3,46	0,765	0,766	3,21	5,75	7,99	3,58	0,34	
10:57:56-11:05:32	1,53	434,2	473,5	256,3	4,27	5,21	16,7	269	3,41	0,773	0,779	3,17	5,53	7,70	3,55	0,42	
11:19:37-11:28:40	1,54	433,8	473,2	259,1	4,18	5,12	16,2	224	3,32	0,781	0,775	3,09	5,30	7,45	3,47	0,35	

Table A.8 Results for the experiment on 17.11.2006

Time	Counter (kWh)	P_1 (kPa)	P_2 (kPa)	P_3 (kPa)	P_4 (kPa)	T_1 (^oC)	T_2 (^oC)	T_3 (^oC)	T_4 (^oC)	m kg/s	T_{in} (^oC)	T_{out} (^oC)	T_{di} (^oC)	T_{do} (^oC)	T_t (^oC)	T_{ci} (^oC)	T_{co} (^oC)
Start 09:08:18	172,78										8,2	5,5					
End 09:22:05	173,11	489	2263	2048	796	32,9	90,1	40,9	13,6	0,0262	13,7	6,1	13,5	36,7	23,3	23,1	23,8
Start 09:43:02	173,13										10,2	11					
End 09:55:01	173,41	545	2469	2445	819	36,4	93,2	42,6	14,3	0,0266	13,9	11,2	13,8	37,1	24,2	24	24,8
Start 14:43:44	173,43										17,7	12,8					
End 14:54:52	173,69	503	2205	2190	808	33,7	89,7	37,5	14	0,0264	21,5	12,5	19,6	40,2	23,8	23,7	24,5
	W (kW)	h_1 (kj/kg)	h_2 (kj/kg)	$h_3=h_4$ (kj/kg)	Q_L (kW)	Q_H (kW)	T_t (^oC)	I (W/m^2)	COP	η_{col}	η_{colth}	COP_{ove}	Q_{Lth} (kW)	Q_{Hth} (kW)	COP_{th}	Q_{us} (kW)	
09:08:18-09:22:05	1,39	441,3	473,1	265,0	4,62	5,45	23,3	336	3,93	0,726	0,765	3,63	7,34	9,40	4,58	0,49	
09:43:02-09:55:01	1,35	443,6	473,6	268,1	4,67	5,47	24,2	403	4,04	0,722	0,787	3,73	7,50	9,52	4,70	0,58	
14:43:44-14:54:52	1,35	441,8	473,5	259,1	4,82	5,66	23,8	403	4,19	0,730	0,792	3,86	7,42	9,44	4,67	0,59	

Table A.9 Results for the experiment on 22.11.2006

Time	Counter (kWh)	P_1 (kPa)	P_2 (kPa)	P_3 (kPa)	P_4 (kPa)	T_1 (^oC)	T_2 (^oC)	T_3 (^oC)	T_4 (^oC)	m kg/s	T_{in} (^oC)	T_{out} (^oC)	T_{di} (^oC)	T_{do} (^oC)	T_t (^oC)	T_{ci} (^oC)	T_{co} (^oC)
Start 11:11:32	173,70										10,4	9,5					
End 11:25:23	174,07	458	2005	1992	718	22	86,6	35,2	9,1	0,0238	15,8	9,5	14,3	36,5	15,8	15,8	16,0
Start 11:44:44	174,09										11,4	9,7					
End 11:55:40	174,38	431	1970	1957	710	20,6	84,8	35,9	8,8	0,0236	16	10	15,7	37,6	15,1	15,1	15,4
Start 12:17:28	174,41										12,8	10,4					
End 12:26:39	174,65	411	1956	1940	708	20,5	84,5	36,8	8,6	0,0235	18,3	11	17,6	38,5	14,7	14,7	15,0
Start 12:45:20	174,67										14	11,2					
End 12:53:57	174,90	447	1978	1964	705	20,3	85,1	36,8	8,4	0,0234	18,9	12,7	17,8	39	14,2	14,2	14,5
Start 15:23:36	174,92										14,6	12,3					
End 15:31:50	175,14	424	1942	1928	702	19,9	84,6	37,3	8,1	0,0232	19,5	11	18,5	39,7	13,6	13,6	13,9
Start 15:49:46	175,16										14,5	10,9					
End 15:58:00	175,38	426	1932	1918	693	19,1	84,1	37,9	7,7	0,0229	19,3	10,8	17,9	38,8	13	13	13,3
Start 16:12:42	175,40										14,2	9,1					
End 16:20:11	175,60	472	1893	1877	674	17,8	81,6	39,0	6,9	0,0224	19,1	8,7	18	38,6	12	12	12,2
	W (kW)	h_1 (kj/kg)	h_2 (kj/kg)	$h_3=h_4$ (kj/kg)	Q_L (kW)	Q_H (kW)	T_t (^oC)	I (W/m^2)	COP	η_{col}	η_{colth}	COP_{ove}	Q_{Lth} (kW)	Q_{Hth} (kW)	COP_{th}	Q_{us} (kW)	
11:11:32-11:25:23	1,55	432,3	472,9	255,0	4,22	5,18	15,8	103	3,34	0,849	0,752	3,11	5,07	7,19	3,40	0,17	
11:44:44-11:55:40	1,54	431,5	471,4	256,2	4,14	5,08	15,1	121	3,29	0,844	0,775	3,07	4,77	6,85	3,29	0,20	
12:17:28-12:26:39	1,52	431,7	471,3	257,8	4,09	5,02	14,7	134	3,31	0,841	0,792	3,07	4,62	6,71	3,21	0,23	
12:45:20-12:53:57	1,55	431,0	471,6	257,8	4,05	5,00	14,2	139	3,22	0,866	0,812	3,00	4,39	6,47	3,11	0,24	
15:23:36-15:31:50	1,55	431,0	471,6	258,7	4,00	4,94	13,6	130	3,18	0,870	0,801	2,96	4,16	6,25	2,99	0,23	
15:49:46-15:58:00	1,55	430,3	471,2	259,7	3,91	4,84	13	112	3,12	0,879	0,802	2,90	4,01	6,09	2,93	0,20	
16:12:42-16:20:11	1,55	428,5	469,1	261,7	3,74	4,65	12	94	2,99	0,930	0,783	2,79	3,86	6,05	2,77	0,17	

Table A.10 Results for the experiment on 23.11.2006

Time	Counter (kWh)	P_1 (kPa)	P_2 (kPa)	P_3 (kPa)	P_4 (kPa)	T_1 (^oC)	T_2 (^oC)	T_3 (^oC)	T_4 (^oC)	m kg/s	T_{in} (^oC)	T_{out} (^oC)	T_{di} (^oC)	T_{do} (^oC)	T_t (^oC)	T_{ci} (^oC)	T_{co} (^oC)
Start 11:11:33	175,64										14,6	12,3					
End 11:28:16	176,08	374	1934	1918	680	18,2	83,4	39,2	7,1	0,0225	21,5	12,1	20	40,1	12,2	12,1	13,4
Start 11:47:32	176,10										15,7	12,2					
End 11:59:19	176,41	369	1918	1903	665	17,4	82,9	39,0	6,7	0,0222	22,3	12,6	20,8	41,5	11,5	11,5	12,9
Start 12:17:42	176,43										15,9	12,9					
End 12:27:35	176,70	575	1885	1872	658	16,7	80,5	37,3	6,3	0,0219	22,4	12,8	21,4	42,6	10,8	10,8	12,4
Start 12:44:26	176,72										16,3	12,8					
End 12:53:57	176,98	600	1769	1754	649	16	78,2	38,0	5,8	0,0217	23,1	12,7	22,6	41,9	10,1	10,1	11,7
Start 13:10:54	177,00										16,1	12,5					
End 13:20:08	177,25	514	1797	1783	642	15,6	79,3	40,6	5,5	0,0215	21,7	12,6	20,8	40,7	9,5	9,5	10,7
Start 13:36:19	177,27										16,5	12,3					
End 13:44:56	177,50	530	1786	1771	637	15,3	78,4	42,1	5,2	0,0210	21,4	12	20,3	40,2	9,0	9,0	9,7
	W (kW)	h_1 (kj/kg)	h_2 (kj/kg)	$h_3=h_4$ (kj/kg)	Q_L (kW)	Q_H (kW)	T_t (^oC)	I (W/m^2)	COP	η_{col}	η_{colth}	COP_{ove}	Q_{Lth} (kW)	Q_{Hth} (kW)	COP_{th}	Q_{us} (kW)	
11:11:33-11:28:16	1,53	430,3	470,4	262,1	3,78	4,69	12,2	627	3,07	0,779	0,825	2,85	3,86	5,95	2,85	0,98	
11:47:32-11:59:19	1,53	429,7	470,1	261,7	3,73	4,63	11,5	671	3,03	0,782	0,827	2,81	3,63	5,78	2,69	1,05	
12:17:42-12:27:35	1,59	426,0	468,0	258,7	3,66	4,58	10,8	716	2,89	0,799	0,828	2,69	3,41	5,48	2,64	1,14	
12:44:26-12:53:57	1,59	425,0	467,2	260,0	3,58	4,50	10,1	707	2,83	0,815	0,829	2,64	3,26	5,34	2,56	1,15	
13:10:54-13:20:08	1,58	426,0	468,0	264,5	3,47	4,37	9,5	537	2,78	0,821	0,832	2,59	3,03	5,13	2,44	0,88	
13:36:19-13:44:56	1,55	425,5	467,2	267,2	3,33	4,20	9	313	2,70	0,803	0,836	2,52	2,88	4,93	2,40	0,50	

APPENDIX B

COMPUTER PROGRAM FOR THE NUMERICAL SIMULATION

B.1 The Efficiency of the Collector

The efficiency of the collector can be simulated with this Mathcad program.

$L := \text{input}$ L, latitude

$n := 1..365$ n, day of the year

$D_n := 23.45 \sin\left[360\cdot(284+n)\cdot\frac{\pi}{(180\cdot 365)}\right]$ D, declination

$T := \text{input}$ T, tilted angle

$i := 1..24$ i, hour of the day

$w(i) := -15\cdot(12-i)$ w, hour angle

$r := \frac{\pi}{180}$

$$R_{b_{n,i}} := \frac{\cos[(L-T)\cdot r]\cdot\cos(D_n\cdot r)\cdot\cos\left[\left(\frac{w(i)+w(i-1)}{2}\right)\cdot r\right]+\sin[(L-T)\cdot r]\cdot\sin(D_n\cdot r)}{\cos(L\cdot r)\cdot\cos(D_n\cdot r)\cdot\cos\left[\left(\frac{w(i)+w(i-1)}{2}\right)\cdot r\right]+\sin(L\cdot r)\cdot\sin(D_n\cdot r)}$$

R_b, the ratio of beam radiation on a tilted surface to a horizontal surface

$$c_{n,i} := \cos(L\cdot r)\cdot\cos(D_n\cdot r)\cdot(\sin(w(i)\cdot r)-\sin(w(i-1)\cdot r)) \qquad d := \frac{12\cdot 3600\cdot 1367}{\pi}$$

$$I_{h_{n,i}} := d\cdot\left(1+0.033\cdot\cos\left(\frac{360\cdot n}{365}\cdot r\right)\right)\cdot\left[c_{n,i}+\frac{\pi\cdot(w(i)-w(i-1))}{180}\cdot\sin(L\cdot r)\cdot\sin(D_n\cdot r)\right]$$

$$I_{0_{n,i}} := \begin{cases} I_{h_{n,i}} & \text{if } I_{h_{n,i}} > 0 \\ 0 & \text{otherwise} \end{cases}$$

I_0, hourly extraterrestrial radiation on a horizontal surface J/m2

$H := input$ H, monthly average daily radiation J/m2

$$w(i) := -15 \cdot \left[12 - \frac{i + (i - 1)}{2} \right]$$ w, hour angle

$$w_{s_n} := acos\left(-tan(L \cdot r) \cdot tan\left(D_n \cdot r\right)\right) \cdot \frac{180}{\pi}$$ w_s, sunset hour angle when Z=90

$$a_n := 0.409 + 0.5016 \cdot sin\left[\left(w_{s_n} - 60\right) \cdot r\right]$$

$$b_n := 0.6609 - 0.4767 \cdot sin\left[\left(w_{s_n} - 60\right) \cdot r\right]$$

$$r_{t_{n,i}} := \frac{\pi}{24} \cdot \left(a_n + b_n \cdot cos(w(i) \cdot r)\right) \cdot \frac{cos(w(i) \cdot r) - cos\left(w_{s_n} \cdot r\right)}{sin\left(w_{s_n} \cdot r\right) - \frac{\pi \cdot w_{s_n}}{180} \cdot cos\left(w_{s_n} \cdot r\right)}$$ r_t, the ratio of hourly to daily radiation

$$I_{n,i} := \begin{cases} H_n \cdot r_{t_{n,i}} & \text{if } H_n \cdot r_{t_{n,i}} > 0 \\ 0 & \text{otherwise} \end{cases}$$ I, hourly total radiation on a horizontal surface J/m2

$$k_{T_{n,i}} := \begin{cases} \overrightarrow{\left(\frac{I_{n,i}}{I0_{n,i}}\right)} & \text{if } I0_{n,i} > 0 \\ 0 & \text{otherwise} \end{cases}$$ k_T, hourly clearness index

$$a_{n,i} := \begin{cases} 1.0 - 0.09 \cdot k_{T_{n,i}} & \text{if } k_{T_{n,i}} \le 0.22 \\ 0.9511 - 0.1604 \cdot k_{T_{n,i}} + 4.388 \cdot \left(k_{T_{n,i}}\right)^2 - 16.638 \cdot \left(k_{T_{n,i}}\right)^3 + 12.336 \cdot \left(k_{T_{n,i}}\right)^4 & \text{if } 0.22 < k_{T_{n,i}} \le 0.8 \\ 0.165 & \text{otherwise} \end{cases}$$

$$I_d := \overrightarrow{(a \cdot I)}$$ I_d, hourly diffuse radiation on a horizontal surface J/m2

$I_b := I - I_d$ I_b, hourly beam radiation on a horizontal surface J/m2

$$I_T := \overrightarrow{(I_b \cdot R_b)} + I_d \cdot \left(\frac{1 + \cos\left(T \cdot \frac{\pi}{180}\right)}{2} \right) + I \cdot 0.35 \cdot \left(\frac{1 - \cos\left(T \cdot \frac{\pi}{180}\right)}{2} \right)$$

I_T, hourly total radiation on a tilted surface J/m2

0.35 is ground albedo.

$T :=$

	1
1	273
2	280
3	300

$c_p :=$

	1
1	4.217
2	4.198
3	4.179

$CS := cspline(T, c_p)$

$fit(x) := interp(CS, T, c_p, x)$

$c_p := fit(T + 273)$ c_p, specific heat of water at temperature T kj/kg.K

$T_i :=$ input T_i, inlet temperature of the fluid to the collector C

$T_o :=$ input T_o, outlet temperature of the fluid from the collector C

$A_c :=$ input A_c, collector area m2

$m :=$ input m, mass flow rate of the water kg/s

$Q_{us} := m \cdot 1000 \cdot c_p \cdot (T_o - T_i)$ Q_{us}, useful energy gain from the collector W

$$\eta_c := \frac{3600 \cdot Q_{us}}{A_c \cdot I_T}$$

B.2 The Performance Characteristics of the Heat Pump

Condensation rate, evaporation rate and COP value of the heat pump can be simulated with this program.

$P_{crit} := 4619$ P_{crit}, critical pressure of the refrigerant R407C kPa

$P :=$ input P, maximum pressure of the refrigerant kPa

$L :=$ input L, length of the evaporator coil m

$D_i :=$ input D_i, inner diameter of the evaporator coil m

$Q_{max} :=$ input Q_{max}, maximum heat transfer at the evaporator W

$q_{max} := \frac{Q_{max}}{\pi \cdot D_i \cdot L}$ q_{max}, maximum heat flux at the evaporator W/m2

$P_r := \frac{P}{P_{crit}}$ P_r, reduced pressure of the refrigerant

$F_p := 1.8 \cdot P_r^{0.17} + 4 \cdot P_r^{1.2} + 10 \cdot P_r^{10}$

$h_i := 0.00417 \cdot q_{max}^{0.7} \cdot P_{crit}^{0.69} \cdot F_p$ h_i, refrigerant side (inner) heat transfer coefficient at the evaporator W/m2K

$T_w :=$ input T_w, temperature of the water in the tank C

$T_e :=$ input T_e, evaporation temperature of the refrigerant C

$T_{av} := \frac{T_w + T_e}{2}$ T_{av}, evaporation temperature of the refrigerant C

$T_f := T_{av} + 273$ T_f, film temperature K

a :=

	1	2	3	4
1	0	0.551	13.67	$1.789 \cdot 10^{-6}$
2	10	0.575	9.52	$1.306 \cdot 10^{-6}$
3	20	0.599	7.02	$1.006 \cdot 10^{-6}$

$T := a^{\langle 1 \rangle}$ T, temperature C $n := rows(a)$

$k := a^{\langle 2 \rangle}$ k, thermal conductivity of the water W/mK

$Pr := a^{\langle 3 \rangle}$ Pr, Prandtl number for water

$\nu := a^{\langle 4 \rangle}$ ν, kinematic viscosity of the water m2/s

Enter degree of polynomial to fit:

$deg := 3$

Number of data points:

$n = 6$

$z := regress(T, ln(Pr), deg)$

$fit(x) := interp(z, T, ln(Pr), x)$

$$k := 0.55097 + 2.26997 \times 10^{-3} \cdot T_{av} + 2.65278 \times 10^{-5} \cdot T_{av}^{2} - 1.28704 \times 10^{-6} \cdot T_{av}^{3} + 1.25 \times 10^{-8} \cdot T_{av}^{4}$$

$$Pr := e^{\left(2.6148 - 0.0391 \cdot T_{av} + 3.21727 \times 10^{-4} \cdot T_{av}^{2} - 1.60663 \times 10^{-6} \cdot T_{av}^{3}\right)}$$

$$\nu := 1.789 \times 10^{-6} - 6.104 \times 10^{-8} \cdot T_{av} + 1.488 \times 10^{-9} \cdot T_{av}^{2} - 2.27 \times 10^{-11} \cdot T_{av}^{3} + 1.5 \times 10^{-13} \cdot T_{av}^{4}$$

$D_o :=$ input D_o, outer diameter of the evaporator coil m

$\beta := \frac{1}{T_f}$ β, thermal expansion coefficient for water 1/K

$$Ra := \frac{\overrightarrow{9.8 \cdot \beta \cdot \left(T_w - T_e\right) \cdot D_o^{3} \cdot Pr}}{\nu^{2}}$$ Ra, Ra number

$$C := \begin{cases} 1.02 & \text{if } 10^{-2} \le Ra_n < 10^{2} \\ 0.85 & \text{if } 10^{2} \le Ra_n < 10^{4} \\ 0.48 & \text{if } 10^{4} \le Ra_n < 10^{7} \\ 0.125 & \text{if } 10^{7} \le Ra_n < 10^{12} \end{cases} \qquad m := \begin{cases} 0.148 & \text{if } 10^{-2} \le Ra_n < 10^{2} \\ 0.188 & \text{if } 10^{2} \le Ra_n < 10^{4} \\ 0.25 & \text{if } 10^{4} \le Ra_n < 10^{7} \\ 0.333 & \text{if } 10^{7} \le Ra_n < 10^{12} \end{cases}$$

$Nu := C \cdot Ra^{m}$ Nu, Nusselt number

$h_o := \dfrac{\overrightarrow{(Nu \cdot k)}}{D_o}$ h_o, water side (outer) heat transfer coefficient at the evaporator W/m2K

$A_i := \pi \cdot D_i \cdot L$ A_i, inner surface area of the coil m2

$A_o := \pi \cdot D_i \cdot L$ A_o, outer surface area of the coil m2

$k_t := input$ k_t, thermal conductivity of the coil tube

$$Q_L := \frac{\overrightarrow{T_w - T_e}}{\dfrac{1}{h_i \cdot A_i} + \dfrac{\ln\left(\dfrac{D_o}{D_i}\right)}{2 \cdot \pi \cdot k_t \cdot L} + \dfrac{1}{h_o \cdot A_o}}$$

Q_L, heat transfer at the evaporator W

$T_{air} := input$ T_{air}, air inlet temperature t othe condenser C

$T_c := input$ T_c, condensation temperature of the refrigerant C

$T_{ave} := \dfrac{T_{air} + T_c}{2}$ T_{ave}, average temperature C

$\lambda_f := \left(93.4 - 0.333 \cdot T_{ave} + 2.23 \cdot 10^{-4} \cdot T_{ave}^{2} - 1.42 \cdot 10^{-5} \cdot T_{ave}^{3}\right) \cdot 10^{-3}$ λ_f, thermal conductivity of the liquid refrigerant W/mK

$\mu_f := \left(218 - 2.83 \cdot T_{ave} + 2.2 \cdot 10^{-2} \cdot T_{ave}^{2} - 1.38 \cdot 10^{-4} \cdot T_{ave}^{3}\right) \cdot 10^{-6}$ μ_f, dynamic viscosity of the liquid refrigerant Pa.s

$c_{pf} := 1.4 + 3.975 \cdot 10^{-3} \cdot T_{ave} + 3.14 \cdot 10^{-5} \cdot T_{ave}^{2} + 9.14 \cdot 10^{-7} \cdot T_{ave}^{3}$ c_{pf}, specific heat of the liquid refrigerant kJ/kgK

$T :=$

	1
1	-70
2	-50
3	-35

$h_f :=$

	1
1	110.1
2	134.2
3	153.2

$h_g :=$

	1
1	370.1
2	383.1
3	392.7

$\rho_{ft} :=$

	1
1	1482.7
2	1413.9
3	1361.3

$\rho_{vt} :=$

	1
1	0.75
2	2.37
3	4.88

$n := 6$

$R := \text{regress}\left[T, (h_g - h_f), n\right]$

$f(x) := \text{interp}\left[R, T, (h_g - h_f), x\right]$

$h_{fg} := \overrightarrow{f(T_c)}$ h_{fg}, latent heat of the refrigerant at condensation temperature kJ/kg

$n := 6$

$R := \text{regress}(T, \rho_{ft}, n)$

$g(x) := \text{interp}(R, T, \rho_{ft}, x)$

$\rho_f := \overrightarrow{g(T_{ave})}$ ρ_f, density of the liquid refrigerant at average temperature kg/m3

$n := 6$

$R := \text{regress}(T, \rho_{vt}, n)$

$h(x) := \text{interp}(R, T, \rho_{vt}, x)$

$\rho_g := \overrightarrow{h(T_c)}$ ρ_g, density of the vapor refrigerant at condensation temperature kg/m3

$h_{fgm} := \overrightarrow{\left[h_{fg} + 0.375 \cdot c_{pf} \cdot (T_c - T_{air})\right]}$ h_{fgm}, corrected latent heat of the refrigerant kJ/kg

$D_{ci} := \text{input}$

$$h_{coni} := \overrightarrow{\left[0.555 \cdot \left[\frac{9.81 \cdot \rho_f \cdot (\rho_f - \rho_g) \cdot h_{fgm} \cdot 10^3 \cdot \lambda_f^{\,3}}{\mu_f \cdot (T_c - T_{air}) \cdot D_{ci}}\right]^{\frac{1}{4}}\right]}$$

h_{coni}, refrigerant side (inner) heat transfer coefficient at the condenser W/m2K

b :=

	1	2	3	4
1	0.0000	0.0244	0.7070	$1.3280 \cdot 10^{-5}$
2	10.0000	0.0251	0.7050	$1.4160 \cdot 10^{-5}$
3	20.0000	0.0259	0.7030	$1.5060 \cdot 10^{-5}$

$T := b^{\langle 1 \rangle}$ T, temperature C

$k := b^{\langle 2 \rangle}$ k, thermal conductivity of the air W/mK

$Pr := b^{\langle 3 \rangle}$ Pr, Prandtl number for air

$\nu := b^{\langle 4 \rangle}$ ν, kinematic viscosity of the air m2/s

Enter degree of polynomial to fit:

deg := 3

z := regress(T, ν, deg)

fit(x) := interp(z, T, ν, x)

$k := 0.02439 + 6.9246 \times 10^{-5} \cdot T_{air} + 4.26407 \times 10^{-7} \cdot T_{air}^{2} - 4.79798 \times 10^{-9} \cdot T_{air}^{3}$

$Pr := 0.70709 - 2.37698 \times 10^{-4} \cdot T_{air} + 1.62338 \times 10^{-6} \cdot T_{air}^{2} - 1.26263 \times 10^{-8} \cdot T_{air}^{3}$

$\nu := 1.32803 \times 10^{-5} + 8.64008 \times 10^{-8} \cdot T_{air} + 1.37554 \times 10^{-10} \cdot T_{air}^{2} + 5.05051 \times 10^{-14} \cdot T_{air}^{3}$

$D_{co} :=$ input D_{co}, outer diameter of the tube at the condenser

$S_T :=$ input S_T, configurarion parameter for tube bank

V := input V, air inlet velocity at the condenser m/s

$V_{max} := \frac{S_T}{S_T - D_{co}} \cdot V$ V_{max}, maximum air velocity at the condenser m/s

$Re_{Dmax} := \frac{V_{max} \cdot D_{co}}{\nu}$ Re_{Dmax}, maximum possible Reynolds number

$2000 < Re_{Dmax} < 40000$ Pr = 0.7

$C := \text{input}$

C and m, constants for airflow over a aligned tube bank of 10 rows

$m := \text{input}$

$Nu_D := C \cdot Re_{Dmax}^{\,m}$ Nu_D, Nusselt number

$h_{cono} := \frac{Nu_D \cdot k}{D_{co}}$ h_{cono}, air side (outer) heat transfer coefficient at the condenser W/m2K

$T_{airout} := \text{input}$

$\overrightarrow{\Delta T_{lm} := \frac{(T_c - T_{air}) - (T_c - T_{airout})}{\ln\left[\frac{(T_c - T_{air})}{(T_c - T_{airout})}\right]}}$ ΔT_{lm}, logarithmic mean temperature difference between tha air and the refrigerant

$L := \text{input}$ L, length of the tube at the condenser m

$A_i := \pi \cdot D_{ci} \cdot L$ A_i, inner surface area of the tube m2

$A_o := \text{input}$ A_o, outer finned surface area of the tube m2

$\overrightarrow{Q_H := \frac{\Delta T_{lm}}{\frac{1}{h_{coni} \cdot A_i} + \frac{\ln\left(\frac{D_{co}}{D_{ci}}\right)}{2 \cdot \pi \cdot k_t \cdot L} + \frac{1}{h_{cono} \cdot A_o}}}$ Q_H, heat transfer at the condenser W

$\overrightarrow{COP := \frac{Q_H}{Q_H - Q_L}}$ COP, coefficient of performance of the heat pump

APPENDIX C

UNCERTAINTY ANALYSIS

"Constant odds combination" method were used to calculate the uncertainties in the experimental study. In this method, if a result R is to be calculated by a function $R=f(x_1, x_2, \ldots x_n)$ from a single set of values of the input data x_i, then the uncertainty in R is given by:

$$w_R = \left[\left(\frac{\partial R}{\partial x_1} w_1 \right)^2 + \left(\frac{\partial R}{\partial x_2} w_2 \right)^2 + \ldots\ldots + \left(\frac{\partial R}{\partial x_n} w_n \right)^2 \right]^{1/2} \qquad \text{(C.1)}$$

where w_n denotes the uncertainty in the n^{th} independent variable.

The second law efficiency of the system can be calculated as follows:

$$\eta_{II} = \frac{A_a + A_w}{A_s + W_c + W_p + W_f} \qquad \text{(C.2)}$$

where A and W denote availability and work respectively. The availabilities of the air, water and solar energy can be evaluated as follows:

$$A_a = m_a \cdot c_{pa} \cdot \left(T_2 - T_1 - T_0 \cdot \ln(\frac{T_2}{T_1}) \right) \qquad \text{(C.3)}$$

$$A_w = m_w \cdot \left(u_2 - u_1 - T_0 \cdot (s_2 - s_1) \right) \qquad \text{(C.4)}$$

$$A_s = \frac{I \cdot A_c}{1000} \cdot \left(1 - \frac{T_0}{T_{effsun}} \right) \qquad \text{(C.5)}$$

where $m_a = \rho_a \cdot V_a \cdot L \cdot h$ and $m_w = \rho_w \cdot v_w$.

The uncertainties in these calculations are determined by the results of the experiments. The values of the variables used in the equations and the uncertainties related to these variables are listed in Table C.1.

Table C.1 Uncertainties of the independent variables.

ρ_a (kg/m^3)	V_a (m/s)	L (m)	h (m)	c_{pa} (kJ/kgK)
1.169±0.023	4.3±0.13	0.8±0.001	0.1±0.0001	1.0035±0.01
T_1 (K)	T_2 (K)	T_0 (K)	ρ_w (kg/m^3)	v_w (m^3/s)
288.3±0.5	311.8±0.5	279.5±0.1	1000±10	0.0002±2x10^{-6}
u_{w1} (kJ/kg)	u_{w2} (kJ/kg)	s_{w1} (kJ/kgK)	s_{w2} (kJ/kgK)	I (W/m^2)
83.1±0.01	68.01±0.01	0.2937±0.0001	0.2419±0.0001	116±5
L_c (m)	w_c (m)	T_{effsun} (K)	W_c (kW)	W_p (kW)
1.7±0.0017	1.2±0.0012	5780±17	1.56±0.05	0.065±0.002
W_f (kW)				
0.050±0.002				

A sample calculation of uncertainty in Equation C.3 is shown as follows:

$$m_a = \rho_a \cdot V_a \cdot L \cdot h = 0.402136 \text{ kg/s}$$

$$\frac{\partial m_a}{\partial \rho_a} = V_a \cdot L \cdot h = 0.344 \qquad w_{\rho_a} = \pm 0.023$$

$$\frac{\partial m_a}{\partial V_a} = \rho_a \cdot L \cdot h = 0.09352 \qquad w_{V_a} = \pm 0.13$$

$$\frac{\partial m_a}{\partial L} = \rho_a \cdot V_a \cdot h = 0.50267 \qquad w_L = \pm 0.001$$

$$\frac{\partial m_a}{\partial h} = \rho_a \cdot V_a \cdot L = 4.02136 \qquad w_h = \pm 0.0001$$

Substituting these values into Equation C.1

$$w_{m_a} = \left[\left(\frac{\partial m_a}{\partial \rho_a} w_{\rho_a} \right)^2 + \left(\frac{\partial m_a}{\partial V_a} w_{V_a} \right)^2 + \left(\frac{\partial m_a}{\partial L} w_L \right)^2 + \left(\frac{\partial m_a}{\partial h} w_h \right)^2 \right]^{1/2}$$

$$w_{m_a} = 0.01452$$

$$A_a = m_a \cdot c_{pa} \cdot \left(T_2 - T_1 - T_0 \cdot \ln(\frac{T_2}{T_1}) \right) = 0.644976$$

$$\frac{\partial A_a}{\partial m_a} = c_{pa} \cdot \left(T_2 - T_1 - T_0 \cdot \ln(\frac{T_2}{T_1}) \right) = 1.603875 \qquad w_{m_a} = \pm 0.01452$$

$$\frac{\partial A_a}{\partial c_{pa}} = m_a \cdot \left(T_2 - T_1 - T_0 \cdot \ln(\frac{T_2}{T_1}) \right) = 0.642726 \qquad w_{c_{pa}} = \pm 0.01$$

$$\frac{\partial A_a}{\partial T_2} = m_a \cdot c_{pa} \cdot \left(1 - \frac{T_0}{T_2} \right) = 0.041804 \qquad w_{T_2} = \pm 0.5$$

$$\frac{\partial A_a}{\partial T_1} = m_a \cdot c_{pa} \cdot \left(\frac{T_0}{T_1} - 1 \right) = -0.012318 \qquad w_{T_1} = \pm 0.5$$

$$\frac{\partial A_a}{\partial T_0} = -m_a \cdot c_{pa} \cdot \ln(\frac{T_2}{T_1}) = -0.031622 \qquad w_{T_0} = \pm 0.1$$

$$w_{A_a} = \left[\left(\frac{\partial A_a}{\partial m_a} w_{m_a} \right)^2 + \left(\frac{\partial A_a}{\partial c_{pa}} w_{c_{pa}} \right)^2 + \left(\frac{\partial A_a}{\partial T_2} w_{T_2} \right)^2 + \left(\frac{\partial A_a}{\partial T_1} w_{T_1} \right)^2 + \left(\frac{\partial A_a}{\partial T_0} w_{T_0} \right)^2 \right]^{1/2}$$

$$w_{A_a} = 0.032688$$

$$\text{Uncertainty (\%)} = \frac{w_{A_a}}{A_a} = 5.07 \ \%$$

If the same procedure is applied to Equations C.4 and C.5, the following table is obtained for the uncertainties in the experimental results.

Table C.2 Uncertainty of the second law efficiency.

	A_a	A_w	A_s	η_{II}
Uncertainty (%)	5.07	7.06	4.31	7